# Neutronic Analysis of Horizontal-Compact High Temperature Gas-cooled Reactor

by

Kristina

B.S., Sriwijaya University (2019)

Submitted to the Department of Nuclear Science and Engineering
in partial fulfillment of the requirements for the degree of

Master of Science in Nuclear Science and Engineering

at the

Massachusetts Institute of Technology

June 2023



Authored by: Kristina
Department of Nuclear Science and Engineering
May 17, 2023

Certified by: Koroush Shirvan
Department of Nuclear Science and Engineering
Thesis supervisor

Certified by: Benoit Forget
Department of Nuclear Science and Engineering
Thesis supervisor

Accepted by: Ju Li
Department of Nuclear Science and Engineering
Chairman, Department Committee on Graduate Theses

This page intentionally left blank

# Neutronic Analysis of Horizontal-Compact High Temperature Gas-cooled Reactor

by

Kristina

Submitted to the Department of Nuclear Science and Engineering
on May 17, 2023, in partial fulfillment of the
requirements for the degree of
Master of Science in Nuclear Science and Engineering

## ABSTRACT

To address the significant cost challenges associated with advanced reactors, a 150MWt horizontal compact high temperature gas-cooled reactor (HC-HTGR) has been proposed. The HC-HTGR has potential to reduce the capital cost of a traditional vertical oriented HTGR by 20% through reduction in reactor building volume. This benefit comes with a trade-off in control system design that requires the usage of control drums due to sagging thin rods in a horizontal layout. Commonly utilized in microreactors, a thorough investigation of control drums must be conducted in reactors with power >100MWt. Parametric studies using OpenMC were carried out to ensure its feasibility. With a uniform enriched core, 12 rotating control drums with an outer radius of 23.4407cm, 0.5cm thickness of 90% enriched $B_4C$, and 0.3cm incoloy cross supports, achieved the highest shutdown margin (SDM) of 3.23%. A sensitivity study on fuel enrichment yielded a SDM of 6.29%, that satisfied the HTGRs design requirement. 2D radial and axial power peaking factor (PPF) with the new enrichment pattern was found at 1.847 and 1.344, respectively. Homogenization using ring reactivity-equivalent physical transformation (RRPT) method was developed to reduce the complexity of the core and showed a good performance with a 4pcm difference in steady-state calculation. Depletion analysis was modeled to ensure the reliability of the new fuel enrichment pattern. The first cycle core sustained criticality for 2.37 years with an average enrichment of 15.5% which meets the design target goal of 2 years cycle length. Overall, the neutronics assessment of HC-HTGR core met the initial safety and design requirements.

Thesis Supervisor: Koroush Shirvan
Title: John Clark Hardwick (1986) Career Development Professor
Professor of Nuclear Science and Engineering

Thesis Supervisor: Benoit Forget
Title: Korea Electric Power Professor of Nuclear Engineering
Department Head, Professor of Nuclear Science and Engineering

# Acknowledgments

I am immensely grateful to my parents for always encouraging my curiosity and enabling me to pursue my dreams. To my siblings, thank you for sharing laughter and annoyance during the most stressful time of my life.

Thank you to my advisors, Koroush Shirvan and Benoit Forget, for their guidance, input, and feedback in shaping the direction of this thesis.

Special thanks to Boston Atomics for the opportunity to contribute to the HC-HTGR concept and for making me part of this decarbonization mission.

Thank you to the entire Nuclear Innovation in Fission Technologies Group and Computational Reactor Physics Group at MIT for their help with this work. Particular thanks to Jiankai Yu and OpenMC community for debugging the HC-HTGR model.

This research made use of the resources of the High Performance Computing Center at Idaho National Laboratory, which is supported by the Office of Nuclear Energy of the U.S. Department of Energy and the Nuclear Science User Facilities under Contract No. DE-AC07-05ID14517.

The work in this thesis was also supported by the Office of Nuclear Energy of the U.S. Department of Energy under the Advanced Reactor Concepts program with Award No. DE-NE0009049.

To all those mentioned above and to those whose contributions may not be explicitly stated, I am deeply thankful for your support. This thesis would not have been possible without each and every one of you. Thank you for being an integral part of my academic journey and for helping me reach this significant milestone.

# Table of Contents

**Table of Contents** **5**

**List of Figures** **7**

**List of Tables** **9**

**1 Introduction** **11**

1.1 Motivation . . . . . 11

1.2 Objectives . . . . . 13

1.3 Outline . . . . . 14

**2 Background** **15**

2.1 TRISO Fuel . . . . . 15

2.2 Burnable Poison . . . . . 17

2.3 Helium Coolant . . . . . 17

2.4 Graphite . . . . . 18

2.5 Control System . . . . . 18

**3 Methods** **20**

3.1 Core Arrangement . . . . . 20

3.2 Control System Modeling . . . . . 23

3.2.1 Control Drums Design . . . . . 23

3.2.2 Control Rods Design . . . . . 24

3.3 Homogenization . . . . . 25

3.4 Design Criteria . . . . . 27
3.5 Computational Implementation . . . . . 28

**4 Result & Discussion** **29**
4.1 Initial Core Performance . . . . . 29
4.2 Control System Analysis . . . . . 30
4.2.1 Control Drums Result . . . . . 30
4.2.2 Control Rods Result . . . . . 33
4.2.3 Control Drums and Inner Control Rods Result . . . . . 35
4.3 Homogenization Assessment . . . . . 36
4.4 Enrichment Variation . . . . . 39
4.5 Depletion Analysis . . . . . 43
4.6 Final Core Performance . . . . . 47

**5 Conclusions** **49**
5.1 Summary of Work . . . . . 49
5.2 Future Work . . . . . 51

**A Detailed Support Design** **52**

**B Fuel Handling Study** **53**

**C Figures** **54**

**D Tables** **58**

**Bibliography** **67**

# List of Figures


1-1 Section view of HC-HTGR building and isometric view of the integrated RPV and SG with RCCS tank [1] . . . . . 13

2-1 TRISO fuel for pebble-bed type and prismatic type HTGRs [2] . . . . 16

3-1 Initial core configuration . . . . . 21
3-2 Fuel block . . . . . 21
3-3 Fuel compact and LBP compact . . . . . 21
3-4 Arc degree variation within cylindrical incoloy . . . . . 24
3-5 Cross incoloy design variation . . . . . 24
3-6 Control rods design variation . . . . . 25
3-7 TRISO and LBP simplification design variation . . . . . 26

4-1 Shannon entropy convergence . . . . . 29
4-2 Enrichment zone . . . . . 40
4-3 Control drums worth as a function of rotation in v3 design . . . . . 42
4-4 Reactivity as a function of burnup and homogeneous design for v0 design. 44
4-5 Nuclides composition as a function of burnup . . . . . 45
4-6 Reactivity as a function of burnup and enrichment variation. . . . . 47
4-7 2D Assembly PPF distribution . . . . . 48

A-1 HC-HTGR control drums with support design . . . . . 52

B-1 Fuel assembly comparison with and without gaps . . . . . 53

C-1 Neutron spectra with 191 energy groups in fuel region for HC-HTGR using final control drums design . . . . . 54
C-2 Neutron flux for various energy groups for HC-HTGR using final control drums design . . . . . 55
C-3 2D Radial pin PPF in core level during criticality for HC-HTGR using final control drums design . . . . . 56
C-4 HC-HTGR model with final control drums design and 2 inner control rods in radial view . . . . . 57

# List of Tables


3.1 Main specification of HC-HTGR . . . . . 22
3.2 Control drums configuration . . . . . 23
3.3 Control rods configuration . . . . . 24
3.4 Homogenization configuration . . . . . 26
3.5 Temperature Distribution . . . . . 27

4.1 Control drums with configuration A . . . . . 31
4.2 Control drums with configuration B . . . . . 31
4.3 Control drums with configuration C . . . . . 32
4.4 Control drums with configuration D . . . . . 32
4.5 Control rods with configuration I . . . . . 34
4.6 Control rods with configuration J . . . . . 34
4.7 Control rods with configuration K . . . . . 35
4.8 Control rods with configuration L . . . . . 35
4.9 Control drums configuration E with incoloy thickness of 0.3cm . . . . 36
4.10 r1m1 design . . . . . 37
4.11 r1m2 design . . . . . 37
4.12 r2m2 design . . . . . 38
4.13 r2m3 design . . . . . 39
4.14 Enrichment zone assignment . . . . . 40
4.15 2D Radial pin PPF of different enrichment pattern . . . . . 41
4.16 2D Radial pin PPF of different enrichment pattern with criticality search 41
4.17 SDM of different enrichment pattern on Control Drums . . . . . 43

4.18 Computation performances . . . . . 46
4.19 Comparison of neutron flux in fuel region with NGNP design . . . . . 48

D.1 Radius of r1m2 homogenization model . . . . . 58
D.2 Control drums with configuration E . . . . . 59
D.3 Control drums with configuration F . . . . . 59
D.4 Control drums with configuration G . . . . . 59
D.5 Control drums with configuration H . . . . . 60
D.6 Additional shutdown from cross hollow . . . . . 60
D.7 Control drums and 4 inner control rods . . . . . 61
D.8 Control drums and 4 inner control rods without outer incoloy . . . . 62
D.9 Control drums and 2 inner control rods . . . . . 63
D.10 Control drums and 2 inner control rods without outer incoloy . . . . 64

# Chapter 1

# Introduction

## 1.1 Motivation

As the average global temperature gradually increased, pledges to achieve net zero emissions by 2050 continue to grow [3]. Nuclear energy has gained great interest in the eye of the public for its carbon-free characteristic to achieve this goal. With 93 operating nuclear power plants (NPPs) in the United States, 62 pressurized water reactors (PWRs), and 31 boiling water reactors (BWRs), nuclear energy contributes to 20% of the nation's electricity generation [4]. Currently, industrial process heat is responsible for 12% of greenhouse gas emissions [5] and is expected to increase for the following years due to projections on population growth. Transition to net zero energy systems cannot be relied solely on producing carbon-free electricity, therefore, a more advanced nuclear reactor that is capable of cogenerating electricity and industrial process heat is preferred to mitigate climate change.

High Temperature Gas-cooled Reactor (HTGR) is one of such concept that has been supported by the Department of Energy (DOE) by launching the next generation nuclear plant (NGNP) program to demonstrate its viability [6, 2]. HTGRs are presently being pursued by many nuclear start-ups due to their high degree of passive safety and technology readiness.

The HTGR design, also known as the second generation of gas-cooled reactors, began in the United Kingdom (UK) when its first experimental reactor, Dragon, went critical in 1964 [7, 8]. With the successful demonstration of the 20MWt prismatic core, the HTGR concept was introduced in the US and led to the first power reactor, Peach Bottom unit 1 operated from 1966 through 1974 [9]. Generating 115MWt power, the Peach Bottom reactor worked well by utilizing bistructural isotropic (BISO) fuels, however, shortcomings in fission product retention arose at higher temperatures [7, 10]. Another layer made from silicon carbide (SiC) was later added to tackle this issue, forming a tristructural isotropic (TRISO) fuel, currently known as the most robust fuel form that provides a high degree of passive safety for several advanced reactor concepts [11]. Following this improvement, a 842MWt reactor at Fort St. Vrain Generating Station was built in 1979 [12]. Until today, 8 HTGRs have been built; AVR and THTR in Germany, HTTR in Japan, HTR-10, and HTR-PM in China. The most recent HTGR with pebble-bed core, HTR-PM, was connected to the grid in December 2021 with a total power of 500MWt [13]. While a proven technology, HTGR has always been criticized for its expensive cost due to requiring a very large building, especially if compared to modern LWR concepts.

In 2020, Stewart et. al. introduced a Horizontal Compact High Temperature Gas-cooled Reactor (HC-HTGR) concept to overcome the high cost [1]. In common HTGRs design, the steam generator (SG) is placed below the reactor pressure vessel (RPV) and connected by a cross vessel to prevent the risk of water ingress. In the horizontal design, the SG and RPV are integrated horizontally into a single flanged vessel, and the cross vessel can be eliminated thus reducing unnecessary space and decreasing the structure volume. A new reactor cavity cooling system (RCCS) is modeled by placing it above and below the RPV with interconnecting pipes to provide a cooling function via radiative heating that reduces the system weight and volume. Since TRISO fuel can also act as a containment system, then reducing the emergency planning zone can increase the geographic options for HTGR sites. HC-HTGR is modularized with outer diameter of RPV at 4.1m. This size makes the RPV transportable thus reducing the shipping cost. Having a horizontal orientation

will make construction faster since the lower stage completion is not needed to start upper stage construction, hence it requires less cost than a vertical orientation. The horizontal concept significantly reduced the overnight civil structure costs by 42%, indirect costs by 38%, and total capital costs by 20% from NGNP, despite operating at lower power rating, and therefore giving the opportunity to HTGR to compete in the energy market.

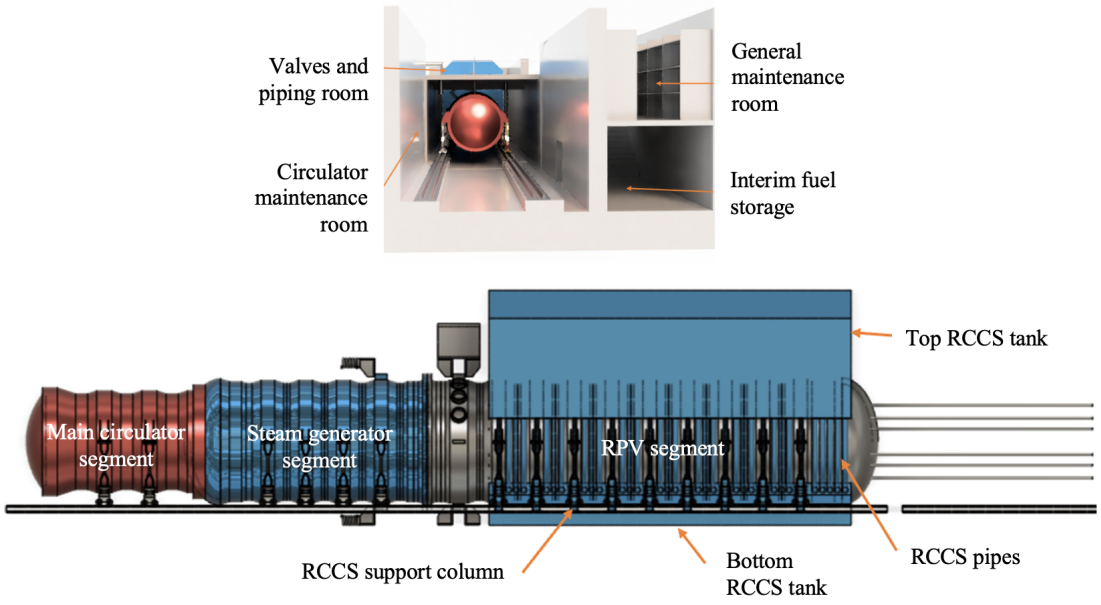


Figure 1-1: Section view of HC-HTGR building and isometric view of the integrated RPV and SG with RCCS tank [1]

## 1.2 Objectives

The focus of this thesis is to mature a 150MWt HC-HTGR concept in terms of the neutronics point of view. The overall design of HC-HTGR will be based on General Atomic's 350MWt prismatic Modular HTGR (MHTGR) [14], one of the NGNP designs. The prismatic version was chosen since it is more amenable to the horizontal orientation than the pebble-bed type design. The Monte Carlo OpenMC code [15] will be used to find the most feasible core design with a control system model that meets neutronics constraints. Steady-state eigenvalue calculations were performed to

obtain initial design parameters. Since the core is expected to be refueled every 24 months, a time-dependent depletion analysis was carried out to ensure its refueling capability. Neutron flux and power distribution were investigated for future work on graphite stress and shielding analysis. Core homogenization was also conducted to reduce modeling complexity.

## 1.3 Outline

Chapter 2 reviews the prior design that has been used to model HTGRs. This includes fuel type, burnable poison, coolant material, and control system design that need to be considered. Chapter 3 describes the test setups of the core modeling including variety of control system design. The detailed homogenization method is also presented. Chapter 4 evaluates the performance of the core and sensitivity tests were analyzed to select the final design. Chapter 5 concludes the work by providing an overall assessment of the HC-HTGR core simulation. Recommendations are made to improve the current model.

# Chapter 2

# Background

## 2.1 TRISO Fuel

TRISO is a type of nuclear fuel that is used in both prismatic and pebble-bed HTGRs. The name TRISO stands for "tristructural-isotropic," which refers to the three coatings that surround the fuel kernels. The outermost and innermost layers are constructed of pyrolitic carbon (PyC), while the middle layer is composed of silicon carbide (SiC). The kernel is typically composed of UCO or $UO_2$ with low enrichment of 5-20%.

One of the key benefits of TRISO fuel is its inherent safety features. The fuel is designed to be extremely resistant to failure, even under extreme conditions. The coatings around the fuel kernels provide a physical barrier that prevents the release of radioactive material in the event of an accident for up to 1600 °C [16]. Additionally, in normal operation, the fuel is designed to operate at high temperatures with a limit of 1250°C, which provides ample margin to the risk of fuel melting and release of radioactive material.

In a prismatic core, fuel regions are arranged in hexagonal prisms that are stacked together to form a core. Each prism contains long cylindrical fuel rods that are made up of thousands of TRISO particles surrounded by graphite. The core is arranged in a cylindrical pressure vessel, and the coolant gas flows through the spaces between the prisms.

In a pebble-bed reactor, the TRISO fuel particles are contained within small tennis ball-sized fuel elements called pebbles. The pebbles are made up of graphite and ceramic coatings that provide structural support and prevent the release of radioactive material. The pebbles are continuously circulated through the core of the reactor by a flow of helium gas.

The HC-HTGR core will be greatly affected by gravity and hence, the pebble-bed type HTGR might introduce greater challenges in fuel handling and maintenance. The prismatic type HTGR offers better design in horizontal layout especially for fuel replacement. It is also capable to operate at high power densities due to the hexagonal fuel that is closely packed, which increases the fuel-to-coolant ratio and improves heat transfer efficiency.

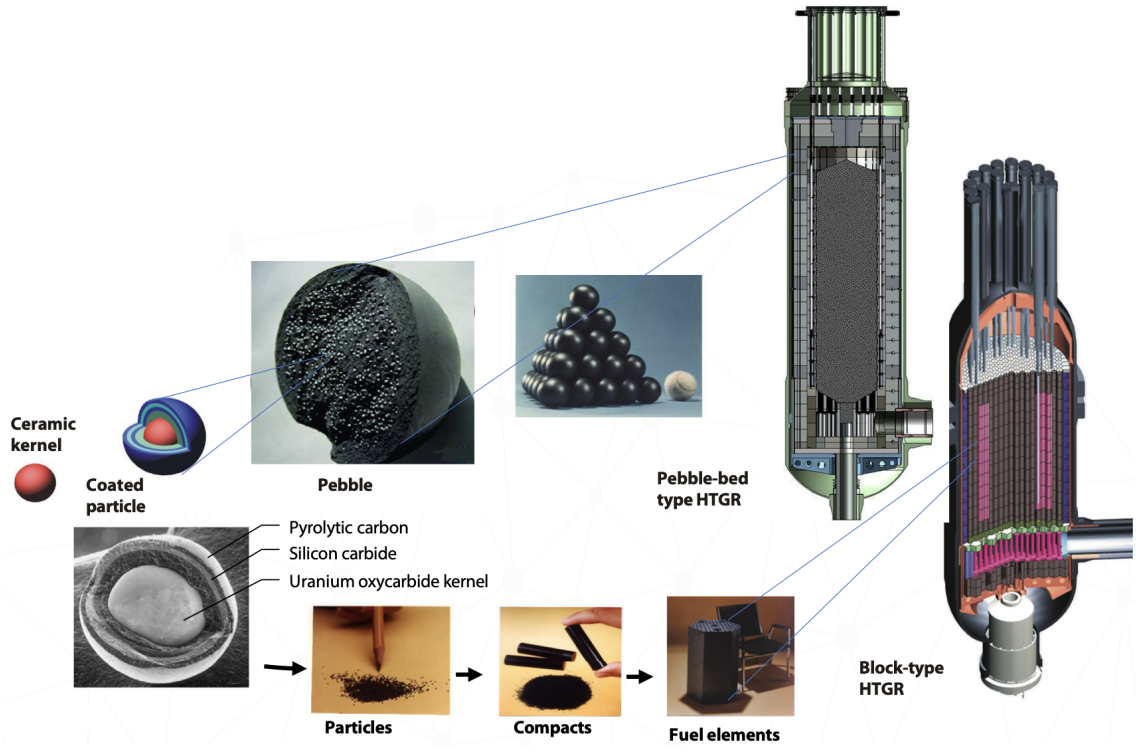


Figure 2-1: TRISO fuel for pebble-bed type and prismatic type HTGRs [2]

## 2.2 Burnable Poison

Burnable poisons are materials that can be added to the fuel elements of HTGR to control the reactivity of the core during operation [14, 17]. It also allows for a more uniform distribution of neutron flux throughout the core, which can improve fuel burnup and reduce the risk of localized hotspots. The most common burnable poison used in HTGR cores is boron carbide ($B_4C$). $B_4C$ has a high neutron absorption cross-section, which means that it is effective at reducing the reactivity of the core. In the prismatic core, burnable poisons are typically designed as granules with PyC coating dispersed in graphite compacts similar to fuel rods.

## 2.3 Helium Coolant

Helium coolant is widely used in HTGRs due to its excellent heat transfer properties and compatibility with high-temperature environments. Helium is a highly efficient coolant, with a thermal conductivity of up to seven times greater than steam [18]. Its low molecular weight and low viscosity allow for efficient heat transfer even at high temperatures, making it ideal for use in HTGRs.

Another advantage of using helium coolant in HTGRs is its chemical stability and non-reactivity. Helium is a noble gas and is chemically inert [17], which means it does not interact with other materials, including nuclear fuel. This property of helium ensures that there is no risk of corrosion or chemical reactions between the coolant and other materials, making it a safer coolant choice. It has a low neutron capture cross-section, which means that it does not absorb neutrons and cause neutron poisoning. Additionally, helium is a non-flammable gas, making it less likely to cause explosions or fire accidents in the reactor. The use of helium as a coolant in HTGRs has been proven to increase reactor efficiency and improve overall safety.

## 2.4 Graphite

Graphite plays a crucial role in HTGRs operation [19, 20]. Serve as a moderator, graphite slows down the fast neutrons produced by the nuclear fission process to efficiently induce further fission reactions. The unique properties of graphite, such as its high melting point, excellent thermal conductivity, and low neutron absorption cross-section, make it an ideal choice for HTGRs. Graphite also acts as a reflector by reflecting the escaping neutrons back into the core, increasing the likelihood of capturing these neutrons by fuel nuclei. This reflection process enhances the overall neutron economy and helps maintain a sustained chain reaction. The combination of graphite as both moderator and reflector in HTGRs contributes to their inherent safety features. Additionally, the low neutron absorption of graphite minimizes the neutron losses, leading to a high fuel utilization and improved reactor efficiency.

## 2.5 Control System

Control rods and control drums are two different components of the control system in nuclear reactors that serve similar purposes, but differ in design and functionality. Both designs are under consideration for HC-HTGR control system.

Control rods are made from thin and long circular cylinder that contain neutron-absorbing material. In a vertical orientation, they are located above reactor vessel and are used by inserting the rods into the reactor core. Control rods are typically used to quickly shut down the reactor in the event of an emergency, as they are capable of absorbing a large amount of neutrons at once. It can also be used to regulate the reactor's power output, by moving the rods up and down.

Commonly used in HTGRs, the control rods have $B_4C$ as the absorber and are covered by metallic material sleeve to support the structure. Incoloy 800H, a nickel-iron-chromium alloy, has been used as support material for HTGR's control rods due to its excellent corrosion resistance and good endurance to high temperatures [21]. The Incoloy 800H was found in Fort St. Vrain, HTR-10, and MHTGR design.

Control drums, on the other hand, have bigger radius than the rods with an annular shape surrounding the fuel region. They also contain neutron-absorbing material that can be rotated to provide a fine-tuned control of the neutron flux distribution in the reactor core, enabling operators to adjust the reactor's power and spatial distribution more precisely.

The inner part of the drums are composed of a reflector material and as described in the previous section, graphite is commonly used in HTGR. Several control drums design use beryllium oxide (BeO) or a combination of beryllium and graphite as reflector due to its superior scattering cross section [22]. However, beryllium also has higher capture cross section compared to graphite, that could reduce the overall neutron economy. It is also a toxic material that poses health and safety concerns [23]. Therefore, beryllium-containing materials where not considered in HC-HTGR control drums design.

Residing within the core periphery, the control drums will absorb some neutrons even when rotated away from the core. As such, control drums tend to be implemented in much smaller reactors like microreactors [24, 25]. Control drums have shown good shutdown performances but data for reactor with power rating >100MWt is currently minimal and require careful study.

Although orientation does not impact the neutronics, switching to a horizontal core introduces new complexities to the control rods management. Control rods are challenging to ensure rapid insertion in horizontal orientation for a 10 m long core due to sagging and insertion channel misalignment. They are also increase space demand to store the rods while operating the core at full power. Therefore, the control drums drive mechanism is suggested as the primary reactivity control and shutdown system in HC-HTGR.

# Chapter 3

# Methods

## 3.1 Core Arrangement

The 150MWt HC-HTGR was developed based on scaling the General Atomics's 350MWt prismatic Modular HTGR (MHTGR) [14]. The core has a cylindrical core consisting of 28 square fuel assemblies with a diameter of 3.2m and an active core length of 8.4m. Graphite reflector with 1m length was added to the front and the back side of the core making up 10.4m in the total length as shown in Figure 3-1.

Instead of using the original hexagonal fuel assembly of MHTGR, the square shape was chosen to enable the piling and moving process in horizontal orientation. The square assembly has a size of $34 \times 34$ cm$^2$ that is stacked horizontally from 12 square fuel blocks. Using the same hexagonal lattice arrangement as MHTGR, the HC-HTGR fuel block consist of 188 fuel rods, 95 coolant rods, and 4 lumped burnable poison (LBP) rods. Each fuel rod has 15 fuel compacts made up of 6,225 TRISO particles while the LBP rod has 14 LBP compacts made up of 46,415 LBP particles. Both fuel and LBP rods have a radius of 0.635cm while coolant rods have radius of 0.795cm.

Figure 3-2 shows the HC-HTGR fuel block arrangement. It can be seen that there are small gaps with size of $1.5 \times 10 \times 50$ cm$^3$ at the lower edge of the block for fuel handling purpose. All void spaces between each rod are filled with graphite as moderator. The main specification of HC-HTGR is presented in Table 3.1.

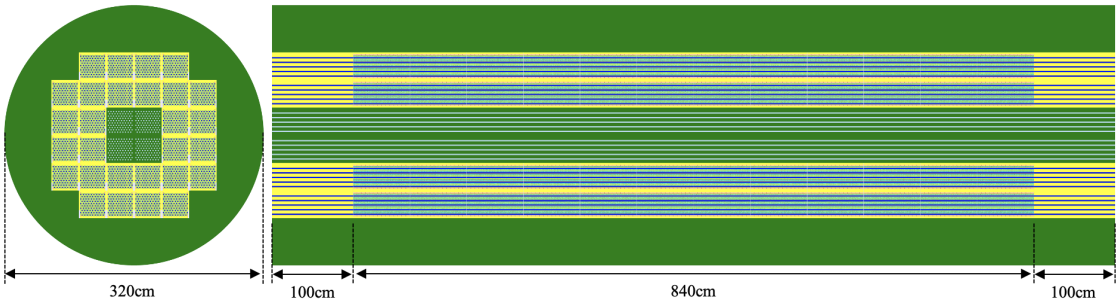


Figure 3-1: Initial core configuration

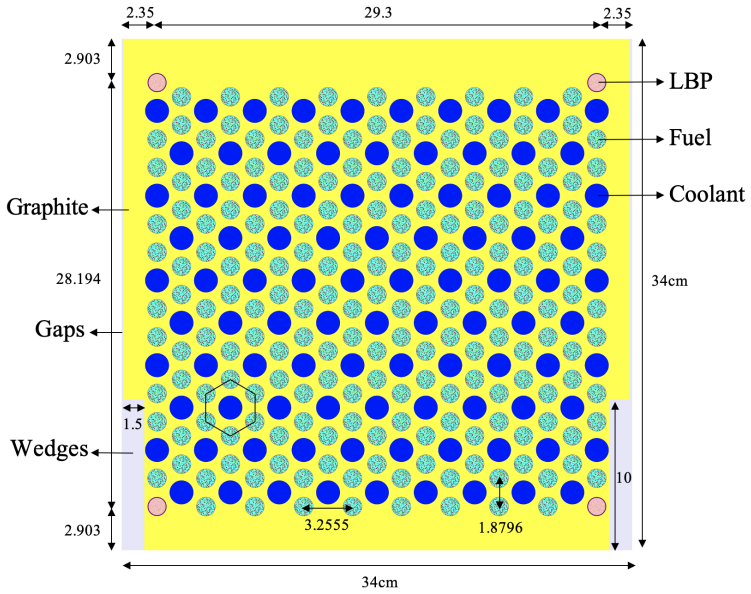


Figure 3-2: Fuel block

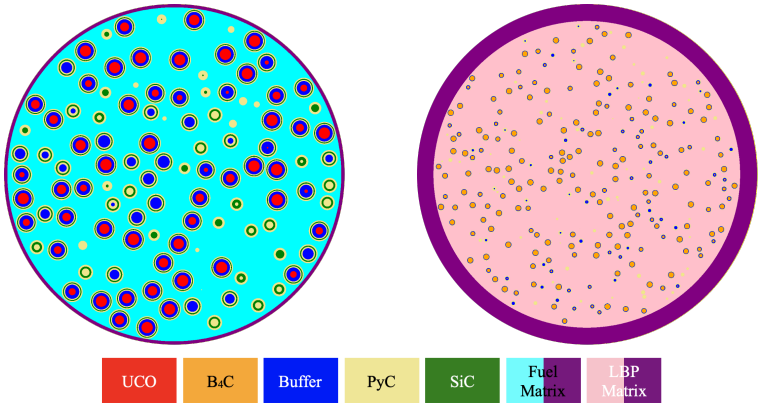


Figure 3-3: Fuel compact and LBP compact

Table 3.1: Main specification of HC-HTGR

| **Core Parameters** | **Value** | **Units** |
|---|---|---|
| Thermal power | 150 | MWt |
| Core power density | 5.93 | $MW/m^3$ |
| Number of fuel columns | 28 | |
| Active core length | 840 | cm |
| Full core length | 1040 | cm |
| Core diameter | 320 | cm |
| Fissile material | $UC_{0.5}O_{1.5}$ | at |
| $U_{235}$ initial enrichment | 15.5 | wt |
| TRISO coating layer materials | Kernel/Buffer/iPyC/SiC/oPyC | |
| TRISO coating layer radius | 212.5/312.5/347.5/382.5/422.5 | $\mu$m |
| TRISO coating layer densities | 10.5/1.0/1.9/3.2/1.9 | $g/cm^3$ |
| TRISO packing fraction | 0.35 | |
| Fuel compact radius/with gap | 0.6225/0.635 | cm |
| Fuel compact graphite density | 1.648 | $g/cm^3$ |
| Primary coolant | Helium | |
| Coolant hole radius | 0.795 | cm |
| Fuel-coolant pitch | 1.8796 | cm |
| LBP coating layer materials | $B_4C$/Buffer/PyC | |
| LBP coating layer radius | 100/118/141 | $\mu$m |
| LBP coating layer densities | 2.47/1.0/1.87 | $g/cm^3$ |
| LBP packing fraction | 0.109 | |
| LBP compact radius/with gap | 0.5715/0.635 | cm |
| LBP compact graphite density | 1.37 | $g/cm^3$ |
| Fuel block size | $34 \times 34$ | $cm^2$ |
| Graphite reflector density | 1.85 | $g/cm^3$ |
| Rod length | 70 | cm |

## 3.2 Control System Modeling

$B_4C$ and Incoloy 800H were used as the main absorber and structural support material for HC-HTGR control system, respectively. Many design parameters can significantly affect the reactivity and therefore, parametric studies on control drums and control rods were carried out to find the most feasible design to shutdown the core.

### 3.2.1 Control Drums Design

Cylindrical horizontal drums with two different radius, 10cm and 23.4407cm, were modeled to test out the reactivity performance. The small radius was used as an initial study while the large one was used to maximize the space throughout the core. The control drums were located in the outer reflector region surrounding the fuel assemblies with 20 small drums and 12 large drums. Both sizes have 4 corner drums that differed from the rest of the drums due to different arc degree. Table 3.2 shows the drums configuration by varying several parameters such as arc degree, incoloy thickness, $B_4C$ thickness, and $B_{10}$ enrichment. Two shapes of the incoloy support; cylindrical and cross, were also modeled to find the best result.

Table 3.2: Control drums configuration

| | **Radius** | **$B_{10}$** | **$B_4C$ Thickness** | **Incoloy** | **Arc Degrees** |
|---|---|---|---|---|---|
| | [cm] | [%] | [cm] | thickness [cm], shape | standard, corner |
| A | 10 | 19.82 | 1.0 | 1.0, cylinder | varied |
| B | 10 | 19.82 | 1.0 | varied, cylinder | 120, 90 |
| C | 10 | 19.82 | varied | 0.5, cylinder | 120, 90 |
| D | 10 | varied | 0.5 | 0.5, cylinder | 120, 90 |
| E | 23.4407 | 90 | 0.5 | varied, Cross1 | 120, 90 |
| F | 23.4407 | 90 | 0.5 | varied, Cross2 | 120, 90 |
| G | 23.4407 | 90 | 0.5 | varied, Cross3 | 120, 90 |
| H | 23.4407 | 90 | 0.5 | varied, Cross4 | 120, 90 |

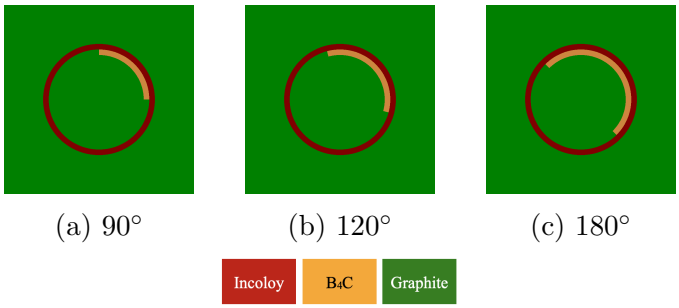


(a) 90° (b) 120° (c) 180°

Figure 3-4: Arc degree variation within cylindrical incoloy

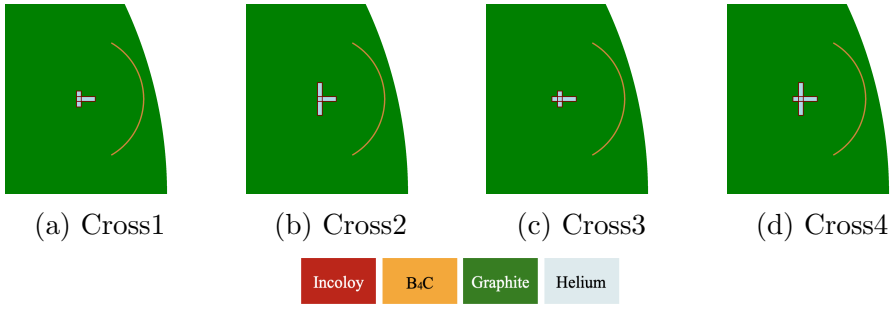


(a) Cross1 (b) Cross2 (c) Cross3 (d) Cross4

Figure 3-5: Cross incoloy design variation

### 3.2.2 Control Rods Design

The control rods were modeled with 20 outer rods and 4 inner rods. There are 2 design; rods with inner incoloy sleeve and rods with both inner and outer incoloy sleeve. The incoloy sleeve thickness was set at a fix value of 0.1cm and was surrounded by a 1.26cm helium gap. The $B_4C$ radius were varied to find the best optimal design. Table 3.3 shows the rods configuration.

Table 3.3: Control rods configuration

| | **Number of Rods** inner, outer | **$B_4C$ Radius** | **Outer Incoloy** |
|---|---|---|---|
| I | 0, 20 | varied | no |
| J | 0, 20 | varied | yes |
| K | 4, 20 | varied | no |
| L | 4, 20 | varied | yes |

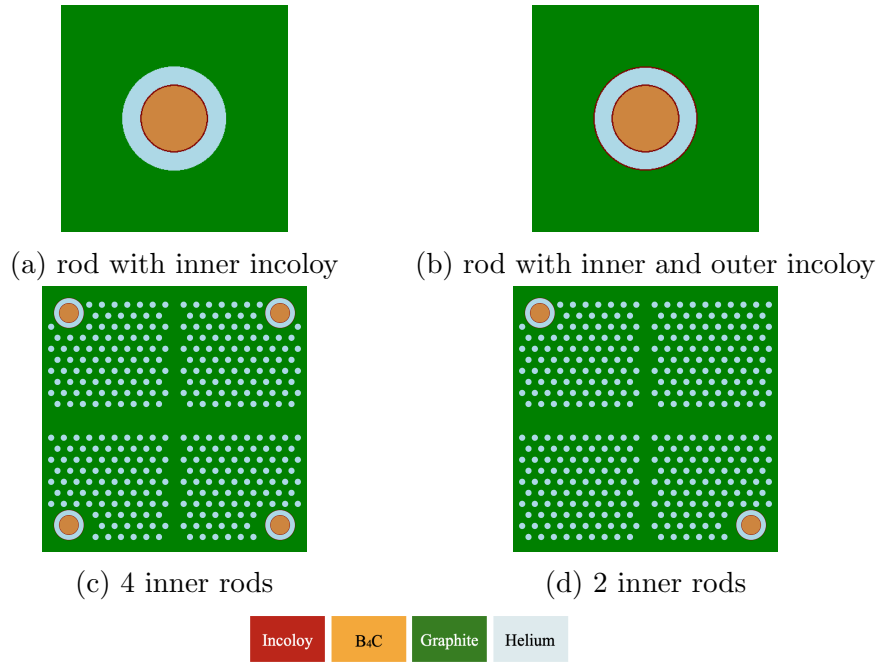


(a) rod with inner incoloy (b) rod with inner and outer incoloy

(c) 4 inner rods (d) 2 inner rods

Figure 3-6: Control rods design variation

## 3.3 Homogenization

The TRISO and LBP configuration lead to double heterogeneity problem, which requires special computational methodology. While Monte Carlo method is able to model the case accurately, it is computationally expensive. The simplest processing method, volume homogenization, has been tested to yield a very large deviation due to self-shielding of dispersed particles. Reactivity-equivalent physical transformation (RPT) method has been proposed by Kim et. al. to tackle this issue [26]. Since the RPT method still has a large deviation for system with dispersed burnable poison particles with large absorption cross section, Loe et. al. improved the RPT method with the ring RPT (RRPT) method and significantly reduce the error [27].

The core homogenization using RRPT method was also being developed in this research to reduce the computational time for time-dependent depletion calculation. Table 3.4 shows the homogenization configuration by varying the number of rings. All configuration has the same outer radius of 0.635cm with length of 8.4m. The ring radius were modified by reactivity search while preserving the material volume. The final design is selected by the smallest $|\Delta k|$ in pcm.

$$\Delta k = (k - k_{ref}) \times 10^5 \tag{3.1}$$

Table 3.4: Homogenization configuration

| | **TRISO region** | **LBP region** | **Matrix region** |
|---|---|---|---|
| r1m1 | 1 | 1 | 1 |
| r1m2 | 1 | 1 | 2 |
| r2m2 | 2 | 2 | 2 |
| r2m3 | 2 | 2 | 3 |

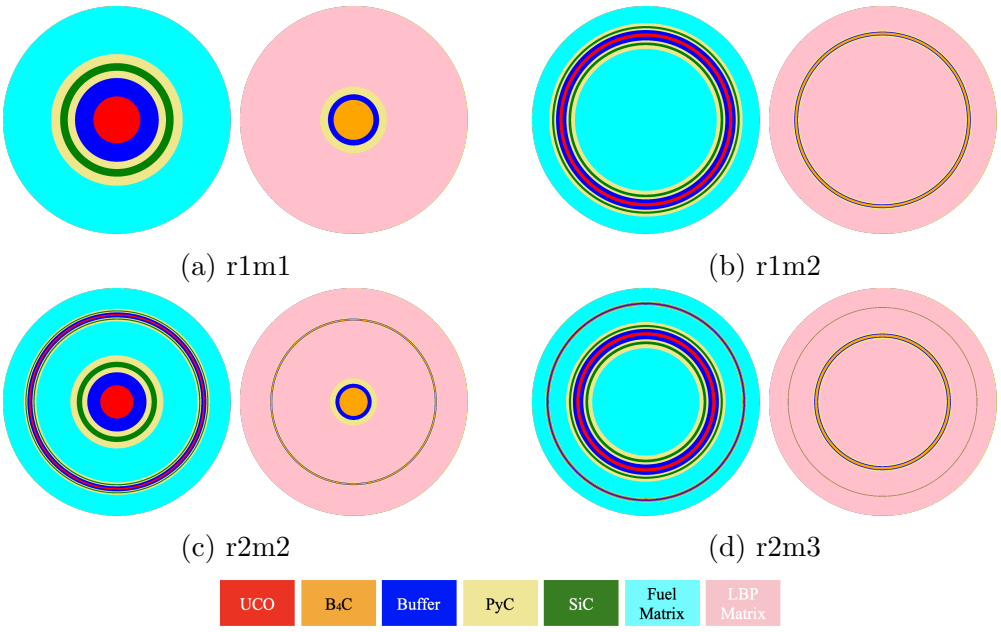


Figure 3-7: TRISO and LBP simplification design variation

For traditional volume homogenization or r1m1 configuration, all TRISO and LBP particles are combined into 1 big cylindrical TRISO and LBP, respectively, and surrounded by graphite matrix. Other configuration with number of ring larger than one has an annular shape with graphite matrix at the inner and outer part. Design of each configuration are shown in Figure 3-7.

## 3.4 Design Criteria

In order to have a subcritical shutdown, the control system design must have a sufficient amount of shutdown margin (SDM). By following the HTGRs operating limit of 1% and reativity swing assumption of 5%, about 6% SDM is desired. The SDM is determined by measuring the reactivity drop between cold zero power (CZP) and hot full power (HFP) conditions when rotating or inserting the neutron absorber. The symbol $i$ and $o$ indicate the control system position in and out, respectively.

$$SDM = [\Delta\rho_1 - \Delta\rho_0] \times 10^{-3} \tag{3.2}$$

$$\Delta\rho_1 = \left[\frac{1}{HFPi} - \frac{1}{HFPo}\right] \times 10^5 \tag{3.3}$$

$$\Delta\rho_0 = \left[\frac{1}{HFPo} - \frac{1}{CZPo}\right] \times 10^5 \tag{3.4}$$

The CZP was set with room temperature condition of $300K$ while HFP was set with operating temperature condition. Table 3.5 shows the operating temperature assignment for different region throughout the HC-HTGR core.

Another aspect of ensuring a safe and efficient nuclear reactor is power peaking factor (PPF). It refers to the ratio of the maximum power density to the average power density within the reactor core. A low power peaking factor is preferred because it indicates that the power is distributed more evenly throughout the core. Taking into account of existing HTGRs design, the HC-HTGR core is targeted to have 2D radial PPF less than or equal to 1.60 and 1.85 for assembly and core level, respectively. A 2D axial PPF of 1.35 is also desired.

Table 3.5: Temperature Distribution

| **Region** | **Operating Temperature** $[K]$ |
|---|---|
| Fuel rods | 1200 |
| LBP rods, coolant channel, graphite blocks | 900 |
| Control system, inner and outer reflectors | 600 |

## 3.5 Computational Implementation

The core modeling and neutronic analysis were carried out using OpenMC, an open-source Monte Carlo neutron and photon transport simulation code [15]. Although the code is relatively young and still under development, it can perform steady-state eigenvalue and time-dependent depletion calculations that have been benchmarked by various widely-used codes. Not only its freely accessible nature, OpenMC uses Python programming interface, a high-level programming language, that enables users to easily understand and implement the model. Another key aspect of choosing OpenMC is its capability of running in parallel using the message passing interface (MPI) that improves simulation time when using large computer systems.

In this study, the ENDF/B-VII.1 continuous-energy nuclear data library generated by NJOY2016 is utilized. As Monte Carlo codes commonly require the number of particle to be set, 200,000 particles with 100 inactive batches and 500 active batches were used throughout this work. Shannon entropy metric was estimated to ensure the convergence of source distribution. Vacuum boundary condition was implemented for the full core simulation.

Benchmark with Serpent, a more mature propriety Monte Carlo reactor physics burnup calculation code [28] was also conducted by the University of Michigan team to verify the research findings.

# Chapter 4

# Result & Discussion

## 4.1 Initial Core Performance

The primary initial assessment of this research is the steady-state eigenvalue calculation, $k$. Initial core performance was measured with the initial core configuration as shown in Figure 3-1 using HFPo condition. OpenMC modeling estimated the core to have $k = 1.10004 \pm 0.00011$. Stationary of the fission source was estimated using Shannon entropy metric. Figure 4-1 shows that the source distribution reached convergence during the inactive batches and remained at a plateau during active batches. To also ensure the reliability of this result, a parallel development of an identical core was performed by the University of Michigan using Serpent and yielded $\Delta k = 150$ pcm. This small difference indicates a good implementation of the model in OpenMC.

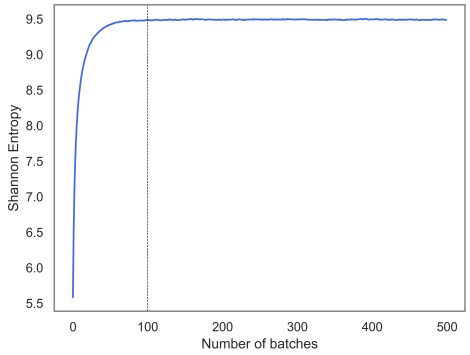


Figure 4-1: Shannon entropy convergence

## 4.2 Control System Analysis

Since the initial reactivity showed a supercritical core, a control system design is required to control the reactor power and ensure safe subcritical shutdown. Both control drums and control rods were designed with several parametric studies using OpenMC as explained in the Table 3.2 and Table 3.3, respectively. Although the previous chapter mentioned the decision of choosing control drums as primary control system of HC-HTGR, analysis of control rods were also conducted to have a better understanding of control system performances.

### 4.2.1 Control Drums Result

In control drums configuration A (Table 3.2), 5 different arc degree were designed. It can be seen in Table 4.1 that all arc degree configuration had a negative SDM and did not satisfy the 6% SDM requirement. This negative result indicates smaller drums worth compared to the cold worth. As expected, the [180,180] configuration gave the lowest SDM due to the lowest drums worth and the highest cold worth. The 180° design has the most amount of $B_4C$ compared to smaller degree and hence absorbed higher amount of reactivity even when the drums were facing away from the core. Since a great amount of neutrons had already been absorbed in HFPo, there was no significant impact when the drums were rotated toward the core. Despite the negative SDM, this arc degree study showed that [120,90] has the most optimal performance with the highest SDM. The resulting arc degree design was later implemented to all other control drums configuration.

In control drums configuration B (Table 3.2), 11 different incoloy thickness were studied. Table 4.2 shows that all incoloy thickness configuration gave a negative SDM and again, did not satisfy the 6% SDM requirement. From the result, we can see that as the incoloy thickness increased, the SDM kept decreasing. This indicates that incoloy contributes to the absorption of neutrons. Since the incoloy support is crucial, and taking into account of the lower impact to the reactivity, the 0.5cm was selected as the final incoloy thickness for further drums analysis.

Table 4.1: Control drums with configuration A

| **Arc Degrees** standard, corner | **CZPo** | **HFPo** | **HFPi** | $\Delta\rho_0$ [pcm] | $\Delta\rho_1$ [pcm] | **SDM** [%] |
|---|---|---|---|---|---|---|
| 180, 180 | 1.10376 | 1.02261 | 1.00437 | 7190 | 1776 | -5.41 |
| 180, 120 | 1.10505 | 1.02406 | 1.00554 | 7157 | 1799 | -5.36 |
| 180, 90 | 1.10563 | 1.02433 | 1.00603 | 7179 | 1776 | -5.40 |
| 120, 120 | 1.10738 | 1.02611 | 1.00644 | 7152 | 1905 | -5.25 |
| 120, 90 | 1.10768 | 1.02693 | 1.00732 | 7099 | 1896 | -5.20 |

Table 4.2: Control drums with configuration B

| **Incoloy Thickness** [cm] | **CZPo** | **HFPo** | **HFPi** | $\Delta\rho_0$ [pcm] | $\Delta\rho_1$ [pcm] | **SDM** [%] |
|---|---|---|---|---|---|---|
| 0.0 | 1.13776 | 1.05465 | 1.00030 | 6926 | 5152 | -1.77 |
| 0.1 | 1.12865 | 1.04737 | 1.00094 | 6876 | 4429 | -2.45 |
| 0.2 | 1.12321 | 1.04211 | 1.00187 | 6929 | 3854 | -3.07 |
| 0.3 | 1.11935 | 1.03820 | 1.00270 | 6983 | 3410 | -3.57 |
| 0.4 | 1.11629 | 1.03535 | 1.00312 | 7003 | 3103 | -3.90 |
| 0.5 | 1.11415 | 1.03315 | 1.00391 | 7037 | 2819 | -4.22 |
| 0.6 | 1.11227 | 1.03147 | 1.00464 | 7043 | 2589 | -4.45 |
| 0.7 | 1.11079 | 1.02997 | 1.00538 | 7064 | 2375 | -4.69 |
| 0.8 | 1.10981 | 1.02877 | 1.00611 | 7098 | 2189 | -4.91 |
| 0.9 | 1.10892 | 1.02744 | 1.00692 | 7151 | 1983 | -5.17 |
| 1.0 | 1.10768 | 1.02693 | 1.00732 | 7099 | 1896 | -5.20 |

In control drums configuration C (Table 3.2), 4 different $B_4C$ thicknesses were modeled. Table 4.3 presents that all $B_4C$ thickness configuration yielded negative SDM and still did not satisfy the 6% SDM requirement. Surprisingly, the SDM remained largely unchanged even after increasing the thickness of $B_4C$. This perfor-

mance provided an opportunity to reduce the HTGR cost by choosing the smallest size of $B_4C$ thickness. Despite the slightly higher SDM in 1.0cm thickness, the 0.5cm was later used in other configurations. The lifetime of this drums was not discussed and will require further study.

Table 4.3: Control drums with configuration C

| **$B_4C$ Thickness** [cm] | **CZPo** | **HFPo** | **HFPi** | **$\Delta\rho_0$** [pcm] | **$\Delta\rho_1$** [pcm] | **SDM** [%] |
|---|---|---|---|---|---|---|
| 0.5 | 1.11463 | 1.03386 | 1.00591 | 7009 | 2688 | -4.32 |
| 1.0 | 1.11415 | 1.03315 | 1.00391 | 7037 | 2819 | -4.22 |
| 2.0 | 1.11302 | 1.03194 | 1.00258 | 7059 | 2838 | -4.22 |
| 3.0 | 1.11211 | 1.03124 | 1.00175 | 7051 | 2855 | -4.20 |

Table 4.4: Control drums with configuration D

| **$B_{10}$** [%] | **CZPo** | **HFPo** | **HFPi** | **$\Delta\rho_0$** [pcm] | **$\Delta\rho_1$** [pcm] | **SDM** [%] |
|---|---|---|---|---|---|---|
| 19.82 | 1.11463 | 1.03386 | 1.00591 | 7009 | 2688 | -4.32 |
| 30 | 1.11441 | 1.03360 | 1.00481 | 7016 | 2772 | -4.24 |
| 40 | 1.11428 | 1.03357 | 1.00372 | 7008 | 2877 | -4.13 |
| 50 | 1.11412 | 1.03334 | 1.00335 | 7017 | 2893 | -4.12 |
| 60 | 1.11428 | 1.03342 | 1.00251 | 7022 | 2984 | -4.04 |
| 70 | 1.11417 | 1.03322 | 1.00238 | 7032 | 2978 | -4.05 |
| 80 | 1.11395 | 1.03311 | 1.00219 | 7024 | 2986 | -4.04 |
| 90 | 1.11404 | 1.03303 | 1.00185 | 7039 | 3013 | -4.03 |
| 100 | 1.11379 | 1.03279 | 1.00155 | 7042 | 3020 | -4.02 |

In control drums configuration D (Table 3.2), 9 different $B_{10}$ enrichment were designed. As shown in Table 4.4, all $B_{10}$ enrichment gave negative SDM and did not

satisfy the 6% SDM requirement. As predicted, the natural boron had the lowest SDM due to the small amount of $B_{10}$ with only 19.82%. The increase in $B_{10}$ led to a corresponding increase in SDM with 100% enrichment gave the highest SDM. However, as the enrichment reached about 60-100% the SDM had only a slight increased.

All small drums design with 10cm radius presented negative SDM which indicates its inability to safely shut down the core and its necessity of selecting larger drum sizes. Outer radius of 23.4407cm was chosen for new configuration to make the most of the available space in the core by meeting the structural constraint of 3cm distance from the core and outer reflector surface. The incoloy support was remodeled into several hollow cross design as shown in Figure 3-5. Similar parametric study without any incoloy support using this larger drums was conducted by the University of Michigan team and resulting on the highest SDM of 4.2% with 90% enrichment of $B_{10}$. By taking this result into account, the 90% $B_{10}$ was used throughout this research.

Similar to the previous result, increasing the thickness of incoloy in the large drums configuration resulting in lower SDM. All cross design yielded much higher SDM but still could not reach the 6% SDM requirement. The highest SDM was obtained at 3.23% from drums configuration E with 0.3cm of incoloy thickness. Performances of control drums configuration E, F, G, and H (Table 3.2) can be seen in Table D.2, Table D.3, Table D.4, Table D.5, respectively.

In addition to increasing the drums worth, the cross hollow was filled with $B_4C$. Table D.6 presents the obtained extra worth from previous design. The thinnest incoloy with the biggest cross design gave the highest worth due to the larger amount of $B_4C$. This additional worth can be used for secondary shutdown mechanism as required for licensing.

### 4.2.2 Control Rods Result

In the control rods study, 8 different $B_4C$ radius were designed. Table 4.5 and Table 4.6 show the SDM performance of configuration I and J (Table 3.3), respectively. Both configuration, regardless of $B_4C$ radius, could not meet the 6% SDM requirement. Configuration J had lower SDM than I due to the presence of outer incoloy that

consumed more neutron during normal operation. Compared to the drums study, the increased of $B_4C$ radius in control rods design gave quite a significant increased.

Since the 20 rods design are still far from the desired SDM, an additional 4 rods were added in the inner reflector region. Table 4.5 and Table 4.6 presents the SDM performance of configuration K and L (Table 3.3), respectively. These extra rods caused the SDM to go up significantly. With and without outer incoloy, both configuration met the 6% SDM requirement even with the smallest $B_4C$ radius of 1.84cm.

Table 4.5: Control rods with configuration I

| **$B_4C$ Radius** [cm] | **CZPo** | **HFPo** | **HFPi** | **$\Delta\rho_0$** [pcm] | **$\Delta\rho_1$** [pcm] | **SDM** [%] |
|---|---|---|---|---|---|---|
| 1.84 | 1.17971 | 1.09771 | 1.01488 | 6332 | 7435 | 1.10 |
| 2.04 | 1.17940 | 1.09756 | 1.01087 | 6322 | 7813 | 1.49 |
| 2.24 | 1.17910 | 1.09708 | 1.00700 | 6341 | 8154 | 1.81 |
| 2.44 | 1.17886 | 1.09680 | 1.00353 | 6347 | 8474 | 2.13 |
| 2.64 | 1.17842 | 1.09650 | 0.99998 | 6340 | 8803 | 2.46 |
| 2.84 | 1.17805 | 1.09602 | 0.99714 | 6353 | 9048 | 2.69 |

Table 4.6: Control rods with configuration J

| **$B_4C$ Radius** [cm] | **CZPo** | **HFPo** | **HFPi** | **$\Delta\rho_0$** [pcm] | **$\Delta\rho_1$** [pcm] | **SDM** [%] |
|---|---|---|---|---|---|---|
| 1.84 | 1.16399 | 1.08434 | 1.01501 | 6311 | 6299 | -0.01 |
| 2.04 | 1.16280 | 1.08346 | 1.01118 | 6298 | 6597 | 0.30 |
| 2.24 | 1.16193 | 1.08225 | 1.00735 | 6336 | 6870 | 0.53 |
| 2.44 | 1.16075 | 1.08136 | 1.00401 | 6325 | 7124 | 0.80 |
| 2.64 | 1.15920 | 1.08030 | 1.00063 | 6300 | 7370 | 1.07 |
| 2.84 | 1.15841 | 1.07913 | 0.99763 | 6342 | 7570 | 1.23 |

Table 4.7: Control rods with configuration K

| $B_4C$ Radius [cm] | CZPo | HFPo | HFPi | $\Delta\rho_0$ [pcm] | $\Delta\rho_1$ [pcm] | SDM [%] |
|---|---|---|---|---|---|---|
| 1.84 | 1.17916 | 1.09720 | 0.90927 | 6335 | 18837 | 12.50 |
| 2.04 | 1.17869 | 1.09678 | 0.89630 | 6336 | 20394 | 14.06 |
| 2.24 | 1.17835 | 1.09635 | 0.88418 | 6347 | 21887 | 15.54 |
| 2.44 | 1.17794 | 1.09590 | 0.87252 | 6355 | 23361 | 17.01 |
| 2.64 | 1.17761 | 1.09565 | 0.86147 | 6352 | 24811 | 18.46 |
| 2.84 | 1.17707 | 1.09524 | 0.85093 | 6347 | 26214 | 19.87 |

Table 4.8: Control rods with configuration L

| $B_4C$ Radius [cm] | CZPo | HFPo | HFPi | $\Delta\rho_0$ [pcm] | $\Delta\rho_1$ [pcm] | SDM [%] |
|---|---|---|---|---|---|---|
| 1.84 | 1.15232 | 1.07428 | 0.90923 | 6304 | 16898 | 10.59 |
| 2.04 | 1.15044 | 1.07260 | 0.89687 | 6308 | 18267 | 11.96 |
| 2.24 | 1.14858 | 1.07096 | 0.88476 | 6310 | 19651 | 13.34 |
| 2.44 | 1.14659 | 1.06909 | 0.87371 | 6322 | 20917 | 14.59 |
| 2.64 | 1.14467 | 1.06753 | 0.86294 | 6313 | 22209 | 15.90 |
| 2.84 | 1.14283 | 1.06562 | 0.85282 | 6340 | 23416 | 17.08 |

### 4.2.3 Control Drums and Inner Control Rods Result

The capability of introducing a very high SDM made inner control rods an attractive control system mechanism. By taking into account the advantages of control drums structure in the horizontal layout, combination of control drums and inner control rods were modeled. The control drums configuration E with incoloy thickness of 0.3cm and control rods with $B_4C$ radius of 2.44cm was selected for this study. By adding control rods hole in the inner reflector, the reactivity in CZPo and HFPo were

slightly lower due to the presence of incoloy sleeve and the absence of some graphite that were supposed to reflect neutron back to the core region. It can be seen that adding 4 inner control rods increased the SDM to 19.23% and went up to 20.27% if outer incoloy sleeve were removed. Since these results are much larger than the requirement, 2 inner control rods were removed. Using only 2 inner rods, the SDM was at 10.87% and 11.46% with and without outer incoloy, respectively. The 6% SDM requirement was met with the drums and inner rods combination. The next several sections will show that the 6% SDM was also met by using control drums alone after enrichment grading. As such, the inner rods mechanism can be used as an emergency shutdown.

## 4.3 Homogenization Assessment

Core homogenization model was developed to increase the performance of the simulation. As mentioned in the previous chapter, the RRPT method was incorporated in this research with 5 different ring design. Table 3.4 presents performances of control drums E configuration with incoloy thickness of 0.3cm in 3 different conditions; full core modeling, full core modeling with support, and $\frac{1}{8}$ core modeling. The incoloy cross design was simplified and thus, the full core modeling with detailed support was carried out to ensure the credibility of the simplification. Detailed support design can be found in Figure A-1.

Table 4.9: Control drums configuration E with incoloy thickness of 0.3cm

| | **CZPo** | **HFPo** | **HFPi** | $\boldsymbol{\Delta\rho_0}$ [pcm] | $\boldsymbol{\Delta\rho_1}$ [pcm] | **SDM** [%] |
|---|---|---|---|---|---|---|
| $\frac{1}{8}$ core | 1.16848 | 1.08646 | 0.98638 | 6461 | 9339 | 2.88 |
| Full core | 1.16698 | 1.08528 | 0.98212 | 6451 | 9678 | 3.23 |
| Full core with support | 1.16741 | 1.08580 | 0.98246 | 6438 | 9687 | 3.25 |

There was no significant difference between full core modeling and full core modeling with support in term of SDM. The $\frac{1}{8}$ core modeling was conducted to have a simpler core with $\frac{1}{4}$ in radial direction and $\frac{1}{2}$ in axial direction. The smaller version of the core came with an over estimated reactivity and slightly lower SDM. Despite this trade-off, the $\frac{1}{8}$ core design was selected as reference case for the homogenization process. It should be noted that 3D temperature profile was not imposed and uniform temperature profile was assumed for all three cases in Table 4.9.

Table 4.10: r1m1 design

| **HFPo** | **Δk** [pcm] |
|---|---|
| 1.32797 | 24151 |

The first homogeneous design was r1m1, the simple volume homogenization method, where the TRISO/LBP region is surrounded with matrix. As expected, the resulting reactivity had a very large deviation.

Table 4.11: r1m2 design

| **Matrix volume** [%] inner:outer | **HFPo** | **Δk** [pcm] |
|---|---|---|
| 40:60 | 1.11085 | 2439 |
| 50:50 | 1.09634 | 988 |
| 55:45 | 1.09017 | 371 |
| 56:44 | 1.08904 | 258 |
| 57:43 | 1.08793 | 147 |
| 58:42 | 1.08670 | 24 |
| 58.1:41.9 | 1.08663 | 17 |
| 58.2:41.8 | 1.08656 | 10 |
| 58.3:41.7 | 1.08621 | -25 |
| 60:40 | 1.08450 | -196 |

The second homogeneous design was r1m2 where the matrix region is divided into two and the TRISO/LBP region is located in the middle. Volume of the inner matrix were adjusted by searching the smallest $|\Delta k|$. With 58.2% of volume in the inner matrix region and 41.8% of volume in the outer matrix region, an error of 10pcm was obtained in the r1m2 design.

Table 4.12: r2m2 design

| **TRISO/LBP volume** [%] inner:outer | **Matrix volume** [%] inner:outer | **HFPo** | **Δk** [pcm] |
|---|---|---|---|
| 10:90 | 50:50 | 1.09789 | 1143 |
| 20:80 | 50:50 | 1.10281 | 1635 |
| 30:70 | 50:50 | 1.11038 | 2392 |
| 40:60 | 50:50 | 1.12050 | 3404 |
| 50:50 | 50:50 | 1.13342 | 4696 |
| 60:40 | 50:50 | 1.15016 | 6370 |
| 50:50 | 40:60 | 1.14251 | 5605 |
| 50:50 | 60:40 | 1.1254 | 3894 |
| 50:50 | 70:30 | 1.11875 | 3229 |
| 50:50 | 80:20 | 1.11313 | 2667 |
| 50:50 | 90:10 | 1.10822 | 2176 |

The third homogeneous design was r2m2 where both TRISO/LBP and matrix region are divided into two. The center part of the rods is the inner TRISO/LBP which is coated with 3 layers; inner matrix, outer TRISO/LBP, and outer matrix. In this design, the volume of the inner TRISO/LBP matrix were adjusted with equal matrix volume to find the smallest $|\Delta k|$. However, Table 4.12 shows high error even though the inner TRISO/LBP region only had 10% of volume. Changing the adjustment to inner matrix volume with constant TRISO/LBP volume still did not improve the result.

Table 4.13: r2m3 design

| **TRISO/LBP volume** [%] inner:outer | **Matrix volume** [%] inner:middle:outer | **HFPo** | **Δk** [pcm] |
|---|---|---|---|
| 40:60 | $\frac{100}{3} : \frac{100}{3} : \frac{100}{3}$ | 1.06786 | -1860 |
| 50:50 | $\frac{100}{3} : \frac{100}{3} : \frac{100}{3}$ | 1.06939 | -1707 |
| 60:40 | $\frac{100}{3} : \frac{100}{3} : \frac{100}{3}$ | 1.07228 | -1418 |
| 70:30 | $\frac{100}{3} : \frac{100}{3} : \frac{100}{3}$ | 1.07761 | -885 |
| 80:20 | $\frac{100}{3} : \frac{100}{3} : \frac{100}{3}$ | 1.08595 | -51 |
| 80.5:19.5 | $\frac{100}{3} : \frac{100}{3} : \frac{100}{3}$ | 1.08650 | 4 |
| 81:19 | $\frac{100}{3} : \frac{100}{3} : \frac{100}{3}$ | 1.08688 | 42 |

The fourth homogeneous design was r2m3 where TRISO/LBP and matrix are divided into two and three regions, respectively. The center part of the rods is the inner matrix which is coated with 4 layers; inner TRISO/LBP, middle matrix, outer TRISO/LBP, and outer matrix. Similar to r2m2, in this design, the volume of the inner TRISO/LBP matrix were adjusted with equal matrix volume to find the smallest $|\Delta k|$. With 80.5% of volume in the inner TRISO/LBP region and 19.5% of volume in the outer TRISO/LBP region, an error of 4pcm was obtained in the r2m3 design.

The r2m3 design gave the most optimal performance and thus, it was chosen as the homogenization configuration in enrichment study.

## 4.4 Enrichment Variation

The enrichment variation study was carried out to obtain 2D radial PPF of 1.6 and 1.85 in assembly and core level, respectively, as well as 2D axial PPF of 1.35 during HFP. In order to find the power distribution of the core, each fuel assembly was divided into 4 regions. The r2m3 homogenization design was used for modeling purpose and thus, making up for 28 total regions. Figure 4-2 and Table 4.14 show the enrichment zone and its enrichment assignment throughout the core.

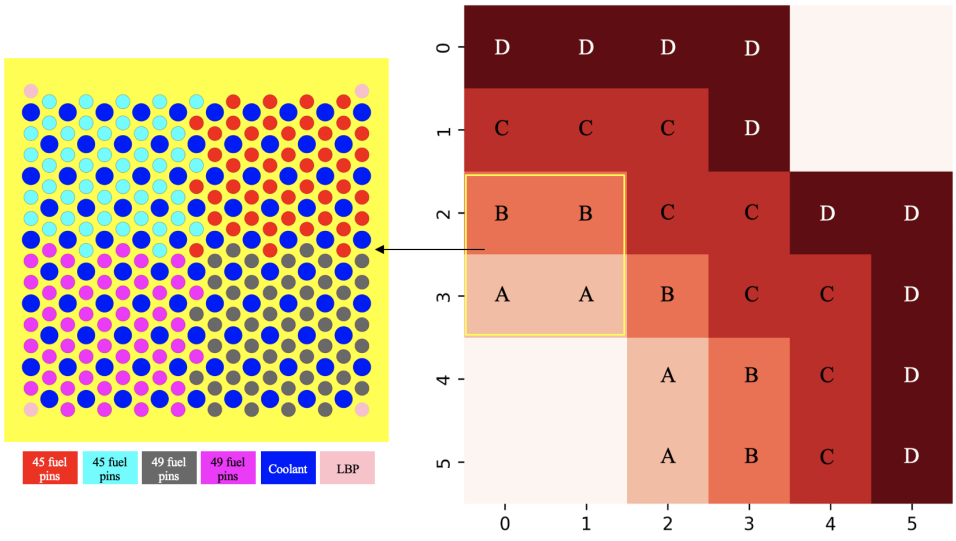


Figure 4-2: Enrichment zone

Table 4.14: Enrichment zone assignment

| **Zone** | **A** | **B** | **C** | **D** | **Average** [%] |
|---|---|---|---|---|---|
| v0 | 15.5 | 15.5 | 15.5 | 15.5 | 15.5 |
| v1 | 9.75 | 12.5 | 17.5 | 17.5 | 15.5 |
| v2 | 9 | 12.5 | 19.5 | 16 | 15.5 |
| v3 | 9.25 | 12.5 | 15.5 | 19.5 | 15.5 |
| v4 | 10 | 13.3 | 17.5 | 17 | 15.5 |
| v5 | 10 | 15.3 | 17.5 | 16 | 15.5 |

The v0 pattern was assigned with uniform 15.5% enrichment and the rest of the pattern was adjusted to match the same average enrichment. The highest peaking location was assigned with lowest enrichment and vice versa.

Resulting assembly and core PPF for each enrichment pattern are presented in Table 4.15. It can be seen that the uniform enrichment pattern had an extremely high PPF. The peak was located at A(2,5) coordinate, based on Figure 4-2, which is right near the inner reflector. This explained the behaviour of the remarkable increased in SDM when inner rods were introduced. All enrichment patterns (v0-v5) yielded

assembly and core PPF below the constraint. These results were not under criticality condition and hence, criticality search was conducted to find the final PPF.

Table 4.15: 2D Radial pin PPF of different enrichment pattern

| | **HFPo** | **Δk** [pcm] | **Assembly** | **Core** |
|---|---|---|---|---|
| v0 | 1.08650 | | 1.859 | 2.384 |
| v1 | 1.06385 | -2265 | 1.572 | 1.615 |
| v2 | 1.06157 | -2493 | 1.523 | 1.526 |
| v3 | 1.06035 | -2615 | 1.522 | 1.529 |
| v4 | 1.06619 | -2031 | 1.570 | 1.657 |
| v5 | 1.06889 | -1761 | 1.516 | 1.668 |

PPF uncertainty $< 0.7\%$

In the criticality search, only two enrichment patterns were studied; v3 and v5. The v3 and v5 patterns had roughly similar performance with v2 and v4, respectively. The v3 pattern was selected due to its high enrichment assignment in zone D instead of in zone C, like v2. In the criticality search, the drums were rotated facing towards the core and will absorb a great amount of neutron near the outer fuel assembly, which is in zone D. This caused the power in that region to be so much lower and by having a very high enrichment in the fuel region that did not get affected with this situation, will rise the peaking factor significantly. The v5 pattern was chosen solely because of its high reactivity compared to v4. The v1 pattern was neglected due to its significant decreased in reactivity but had relatively the same PPF as v5.

Table 4.16: 2D Radial pin PPF of different enrichment pattern with criticality search

| | **Drums rotation** | **HFPo** | **Assembly** | **Core** |
|---|---|---|---|---|
| v3 | 94° | 1.00024 | 1.573 | 1.847 |
| v5 | 107° | 1.00048 | 1.570 | 2.066 |

PPF uncertainty $< 0.7\%$

Criticality search in OpenMC modeling required iteration of simulation per drums rotation. By rotating the drums 94° counter clockwise towards the core, the v3 pattern reached criticality with pin PPF of 1.573 and 1.847 in the assembly and core level, respectively, as listed in Table 4.16. These results met the pin PPF limitation for HC-HTGR. The v5 pattern reached criticality with 107° rotation and resulted pin PPF of 1.57 and 2.066 in the assembly and core level, respectively. The pin PPF constraints cannot be reached with v5 pattern. Figure 4-3 shows the control drums worth as a function of rotation in v3 design.

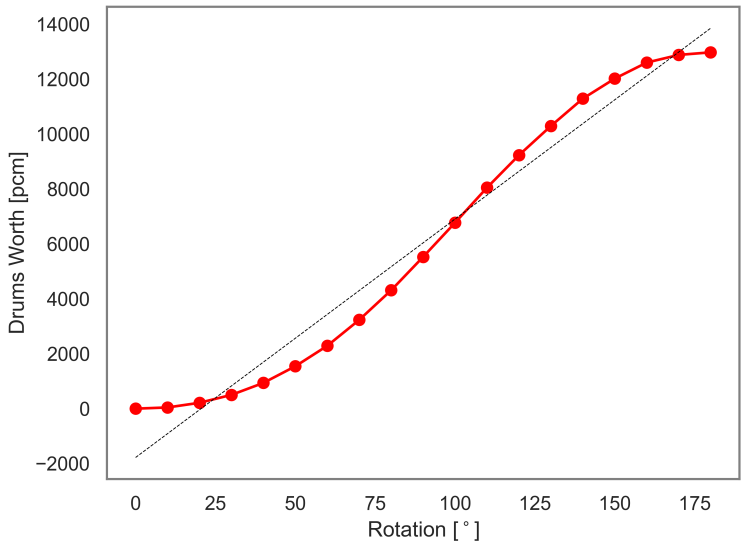


Figure 4-3: Control drums worth as a function of rotation in v3 design

Changing the enrichment pattern requires new calculation of SDM. Table 4.17 presents the SDM performance of every enrichment pattern. It can be seen that the SDM increased for all the enrichment pattern and the v3 pattern had the highest SDM that finally satisfied the 6% requirement. This v3 pattern was later implemented for time-dependent depletion analysis.

Table 4.17: SDM of different enrichment pattern on Control Drums

| | **CZPo** | **HFPo** | **HFPi** | $\boldsymbol{\Delta\rho_0}$ [pcm] | $\boldsymbol{\Delta\rho_1}$ [pcm] | **SDM** [%] |
|---|---|---|---|---|---|---|
| v0 | 1.16775 | 1.08650 | 0.98607 | 6404 | 9374 | 2.97 |
| v1 | 1.14706 | 1.06385 | 0.93995 | 6819 | 12390 | 5.57 |
| v2 | 1.14445 | 1.06157 | 0.93827 | 6822 | 12379 | 5.56 |
| v3 | 1.14352 | 1.06035 | 0.93061 | 6859 | 13148 | 6.29 |
| v4 | 1.14907 | 1.06619 | 0.94526 | 6765 | 11999 | 5.23 |
| v5 | 1.15161 | 1.06889 | 0.95298 | 6720 | 11379 | 4.66 |

## 4.5 Depletion Analysis

In order to ensure a 24-month refueling scheme in HC-HTGR is viable, depletion analysis must be conducted. Since the selected v3 pattern used the r2m3 homogenization method, its reliability for time-dependent depletion analysis must be verified. Taking into account the r1m2 homogenization method that showed great performances as much as r2m3, its depletion model was also simulated. The depletion calculations were carried out with v0 enrichment pattern as an initial performance comparison.

From Figure 4-4, we can see that the homogenization method in HC-HTGR core performed greatly in the beginning of life but had higher error after several hundreds days. Both r1m2 and r2m3 models gave similar error pattern that under estimated the reactivity during middle of life and over estimated the reactivity at the end of life. The r1m2 model showed a relatively smaller error compared to r2m3 with negative peak at 68pcm after 3.16 years of operation and positive peak at 93pcm after 5.67 years of operation. The r2m3 had negative peak at 389pcm after 2.16 years of operation and positive peak at 187pcm after 6 years of operation. Overall, the depletion performance in homogenization design is relatively good for 24 months. The r1m2 and r2m3 gave an average error of 25 and 151pcm, respectively.

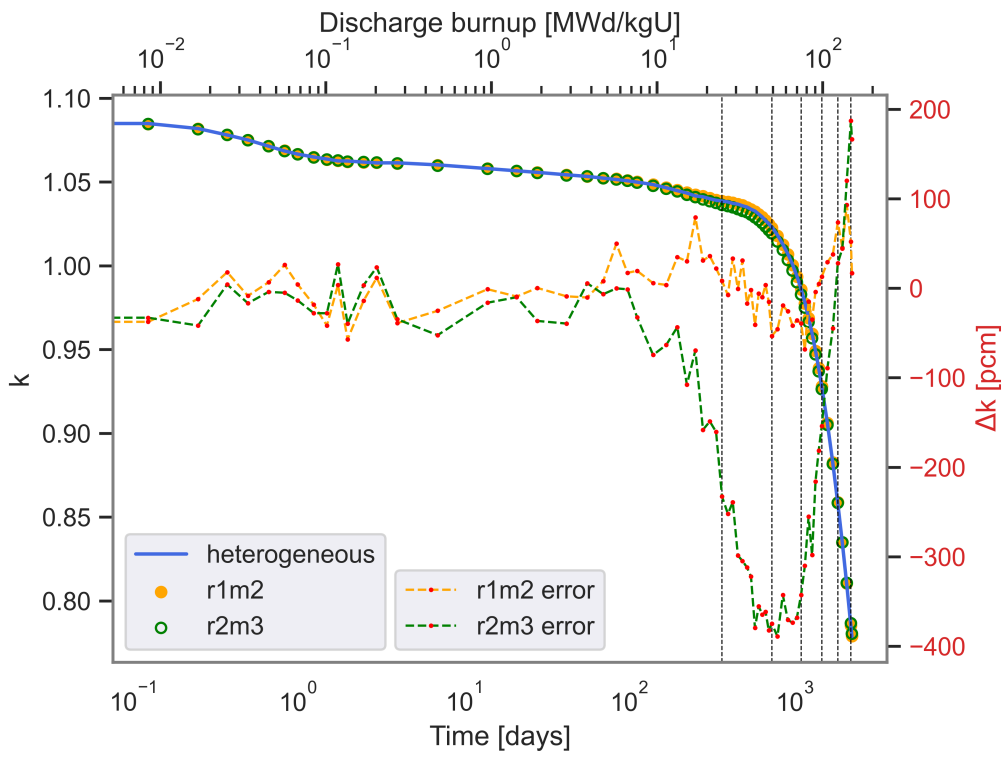


Figure 4-4: Reactivity as a function of burnup and homogeneous design for v0 design.

To understand the reasoning behind the deviation in the homogenization method, number of atoms from several isotopes were plotted and compared to the heterogeneous one. As shown in Figure 4-5, the composition of $U_{235}$ was similarly approximated throughout the core but $B_{10}$ was slightly over estimated. Although the difference was small, this indicates the reason of the under estimation of the homogenization methods during the middle of life. The core was depleting $B_{10}$ slightly slower than it should be and caused the $B_{10}$ to absorb more neutrons and yielded lower reactivity. This behavior is suspected to be from the division of LBP region, where the slow burning process happened at the inner layer. Radioisotopes like $Pu_{239}$ and $Pu_{241}$ were also evaluated and the composition was found to be also slightly over estimated. The r2m3 model tended to have higher composition than r1m2 which was expected due to higher error in the depletion calculation. The $Xe_{135}$ and $I_{135}$ build-up were observed during the first 4 days and both models align precisely with the heterogeneous design.

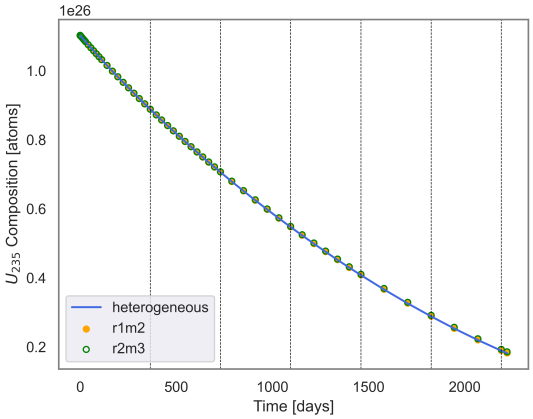


(a) Number of $U_{235}$ atom in fuel

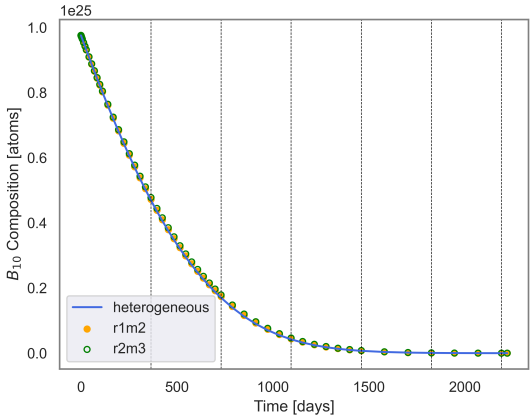


(b) Number of $B_{10}$ atom in LBP

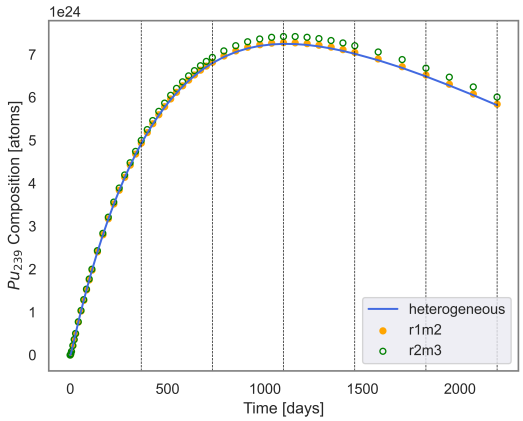


(c) Number of $Pu_{239}$ atom in fuel

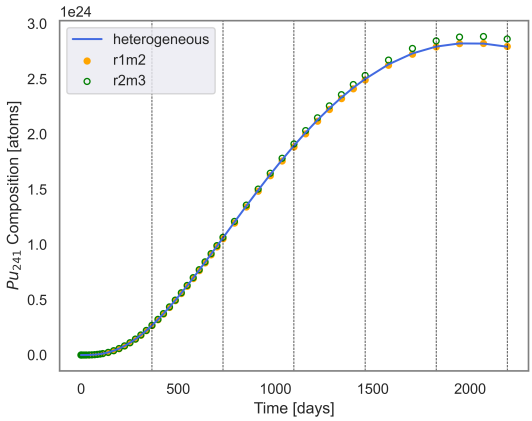


(d) Number of $Pu_{241}$ atom in fuel

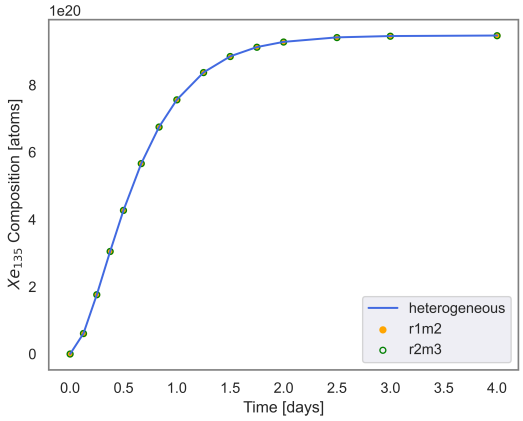


(e) Number of $Xe_{135}$ atom in fuel

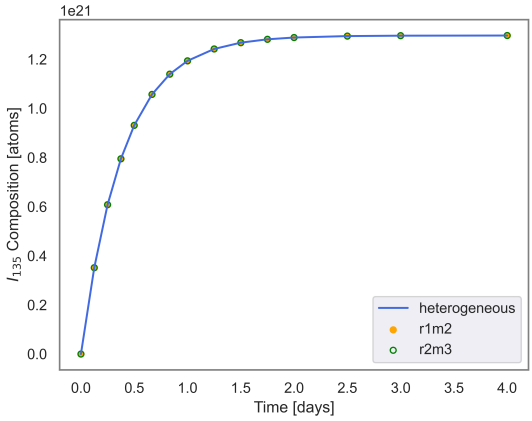


(f) Number of $I_{135}$ atom in fuel

Figure 4-5: Nuclides composition as a function of burnup

Runtime comparison between homogeneous and heterogeneous designs can be seen in Table 4.18. With using half as much processor as the heterogeneous model, the r1m2 and r2m3 models ran 1.8 and 1.4 times faster. After each OpenMC calculation, an output of HDF5 file, summary.h5, was generated as a complete description on the geometry and materials used in the simulation. The size of summary.h5 was measured to know the simplicity of the homogeneous model. As predicted, the file size was so much smaller with only a couple of MB, compared to the heterogeneous model with about 8GB, which was due to the disappearance of TRISO particles. The r1m2 ran slightly faster and had smaller file size than the r2m3 model because of the smaller number of rings. Since the r1m2 model gave better depletion performances, it can be used as future homogenization method in HTGRs.

Table 4.18: Computation performances

| | **Number of processor** | **Runtime** [hours] | **Size of summary.h5** [MB] |
|---|---|---|---|
| r1m2 | 60 | 35.83 | 3.35 |
| r2m3 | 60 | 47.39 | 4.69 |
| heterogeneous | 120 | 64.68 | 8411.59 |

Although the homogenization performance for v0 pattern was relatively good, the depletion analysis for v3 was conducted using heterogeneous design. Figure 4-6 presents the reactivity of v0 and v3 pattern over 6 years of operation. The v3 pattern reached criticality with all drums out at 2.37 years with discharge burnup of 58.43MWd/KgU. As anticipated, the v3 fuel stays critical for a shorter time compared to v1 fuel which was critical until 2.69 years. The depletion analysis showed that the v3 core can sustain a 24 months fuel cycle for the first core.

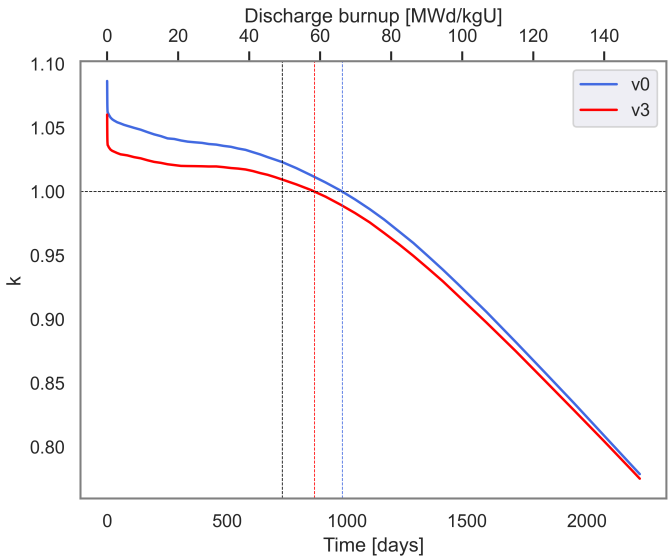


Figure 4-6: Reactivity as a function of burnup and enrichment variation.

## 4.6 Final Core Performance

This section evaluates the performances of the v3 core design. Three different energy range; thermal (E $<$ 0.625 eV), intermediate (0.625 eV $<$ E $<$ 0.1 MeV), and fast (E $>$ 0.1 MeV), were used to observe the neutron flux throughout the core. 191 energy groups were also used to understand the neutron flux within the fuel region. Additionally, radial and axial PPF were discussed later in this section.

The neutron flux distribution can be seen in Figure C-2. The fast and intermediate flux mostly occupied the fuel assemblies due to the high energy neutrons produced from fission reactions. The thermal flux was located in the reflector regions, with peak in the inner reflector, because there was no source of higher energy neutrons. Fast neutrons that traveled from fuel region were moderated or reflected back by graphite.

Using 191 energy groups, neutron flux within fuel region was observed. As shown in Figure C-1 the neutron peak was 2.59 $\times 10^{12}$ n.cm$^{-1}$.s$^{-1}$ within energy of 0.112-0.146 eV while the total flux was about 10.508 $\times 10^{13}$ n.cm$^{-1}$.s$^{-1}$. Flux comparison between 150MWt HC-HTGR and 600MWt NGNP are presented in Table 4.19.

Table 4.19: Comparison of neutron flux in fuel region with NGNP design

| **Upper bound energy** [MeV] | **Neutron flux** [$10^{13}$ n.cm$^{-1}$.s$^{-1}$] | |
|---|---|---|
| | 600MWt NGNP [29] | 150MWt HC-HTGR |
| 1.4 $\times 10^{-6}$ | 7.808 | 2.520 |
| 0.1 | 6.769 | 5.356 |
| 20 | 3.475 | 2.632 |
| Total | 18.052 | 10.508 |

In the previous section, the pin PPF has been evaluated hence in this section, the assembly PPF is going to be assessed. It can be seen in Figure 4-7, that the radial assembly PPF was smaller compared to pin PPF. Each assembly had roughly the same power with average of 5.4MWt for the full core length. The axial PPF was found to be 1.344 at the center of the core, which satisfied the HC-HTGR design target based on preliminary considerations. A closer look of pin PPF throughout assembly at coordinate (1,2), based on Figure 4-7, can be found in Figure C-3.

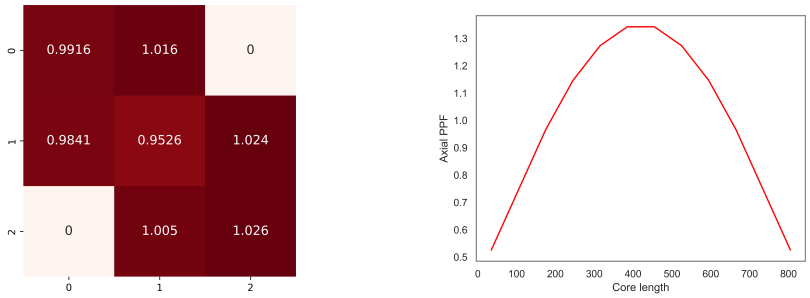


(a) Radial PPF (b) Axial PPF

PPF uncertainty $< 1.0\%$

Figure 4-7: 2D Assembly PPF distribution

# Chapter 5

# Conclusions

## 5.1 Summary of Work

The implementation of HC-HTGR can offer economic benefits by decreasing the required building volume and streamlining the construction process. Nevertheless, the transition to a smaller horizontal design could create challenges in the control systems design and reactor power management. This aspect has been cafefully examined in order to improve the design of HC-HTGR.

Parametric studies have been conducted for control drums and control rods design. Two control drums sizes were modeled to investigate the SDM performance. Both small and large drums were not able to meet the SDM requirement. The highest SDM was found at 3.23% from large control drums using cross1 incoloy design with thickness of 0.3cm. The control rods design also could not reach the 6% SDM but, adding 4 rods in the inner reflector significantly boost the SDM and finally satisfied the design criteria. Combination of control drums and inner control rods were tested, and as anticipated, this combination performed very well with a very high excess margin. By using only 2 inner rods, the design had SDM of 11.466% and 10.87% for rods with and without outer incoloy, respectively.

However, control rods are not desirable in the horizontal layout. Instead, the inner control rods design could be an attractive emergency shutdown system. Since the inner reflector had a great impact in the reactivity, power peaking assessment was

carried out to understand the power distribution of the core. This information was later used to select an appropriate enrichment pattern to evenly distribute power.

The power peaking assessment was conducted in critical core condition that requires a lot of iteration. Modeling with OpenMC and all other stochastic codes is highly expensive especially for reactor with dispersed particles; TRISO and LBP. To reduce the computation time, homogenization process was carried out based on RRPT method [27]. The r2m3 methods (Table 3.4) gave the most optimal result with only 4pcm difference with heterogeneous core in HFPo condition. The method divided TRISO/LBP and graphite matrix into two and three rings, respectively, with inner matrix as the center and was coated with 4 layers; inner TRISO/LBP, middle matrix, outer TRISO/LBP, and outer matrix.

Implementing the r2m3 homogenization, the power peaking was evaluated for uniform 15.5% enrichment, v0. While not in the critical condition, the core had an extremely high peak near inner reflector with 1.859 and 2.384 for assembly and core level, respectively. To tackle this issue, each fuel assembly was divided into 4 region and each region was assigned with different enrichment according to the power peaking level of its region. The PPF requirement was reached by using enrichment pattern v3 (Table 4.14). In the critical core, radial pin PPF was found at 1.573 and 1.847 in assembly and core level, respectively. This low peaking improved the control drums worth and yielded a SDM of 6.29% by only using control drums. This v3 pattern was selected as the final enrichment of HC-HTGR core.

Time-dependent depletion analysis was conducted to ensure the capability of v3 design to remain critical for over 24 months with the initial core loading. A depletion calculation using v0 enrichment pattern with two homogeneous cores, r1m2 and r2m3 (Table 3.4), were performed along with heterogeneous core. The homogeneous core had a similar performance at the beginning of life but under estimated the reactivity throughout the end of life. The r1m2 design showed the best optimal homogenization with two peak error of -68pcm at 3.16 years and 93pcm at 5.67 years. With runtime about 1.8 times faster by using half amount of processors, the r1m2 model can be used for future HTGR modeling. Depletion analysis for v3 design was later performed

and showed its criticality at 2.37 years with discharge burnup of 58.43MWd/Kg.

Given the results that have been found, the control system and enrichment loading proposed for the HC-HTGR meets the reactor physics design targets. With the growing popularity of nuclear energy as a means to reduce carbon emissions in energy production, the HC-HTGR could offer an affordable and secure option. Multiple studies have been conducted, and are currently ongoing, to ensure that the HC-HTGR is ready for licensing and eventual deployment through a multidisciplinary approach.

## 5.2 Future Work

During the course of this study, numerous assumptions and simplifications were essential for constructing this initial core model. Consequently, there is substantial scope for enhancing the model in the future. Although there are several avenues for improvement, a handful of recommendations are presented herein that could considerably enhance the underlying assumptions of this model.

- Study on one stuck rod/drum to ensure capability of shutdown even if one control rod/drum is completely removed from the reactor.
- Perform core shuffle and reload analysis to find attainable core cycle length for designs within 150-200 MWt.
- Ensure drums lifetime by looking at depletion of drums.
- Reactor kinetics analysis.
- Adding barrel, RPV structures, and the outer part of the reactor for more detailed design.
- Implement axial temperature profile for fuel, coolant, and graphite.
- Coupling with thermal hydraulics codes to obtain effect of thermal feedback

# Appendix A

# Detailed Support Design

In horizontal orientation, control drums design face a challenging aspect due to gravity force. Drums that are located at the lower part of the core might be experiencing extra weight and pressure which require additional structural support. Here are the detailed support design needed in control drums model.

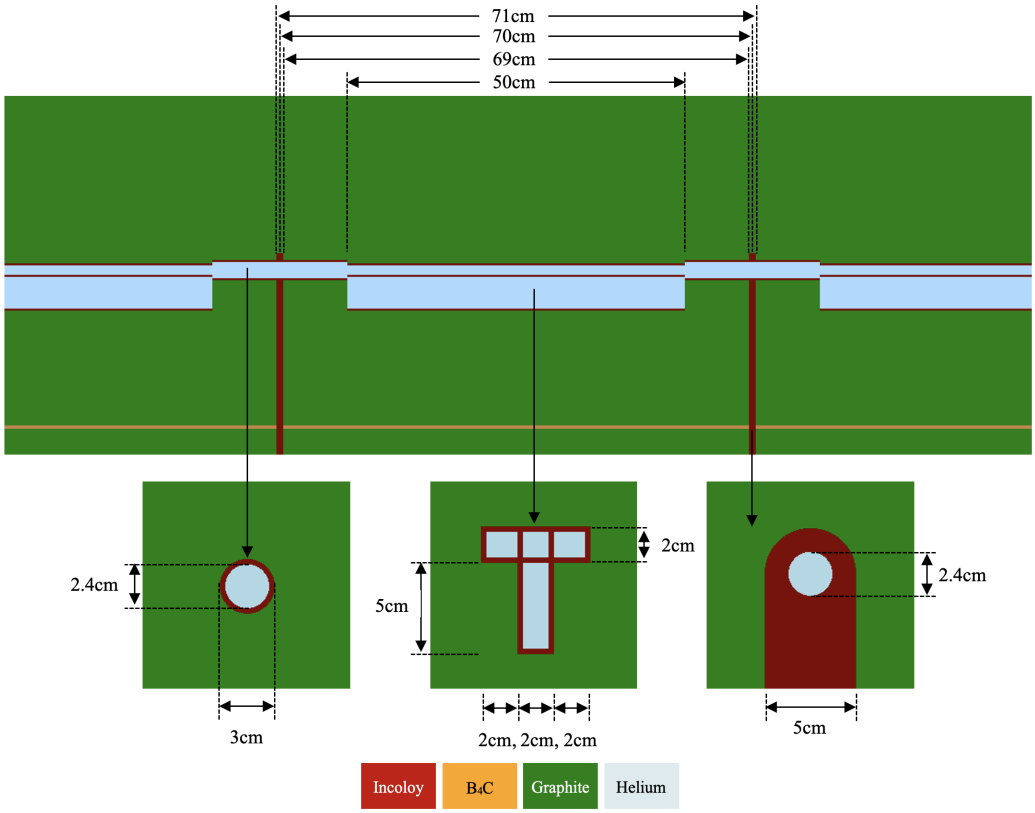


Figure A-1: HC-HTGR control drums with support design

# Appendix B

# Fuel Handling Study

Throughout this research, fuel handling holes; gaps and wedges, were included in the design as shown in Figure 3-2. Comparison study was carried out to understand the impact of replacing the holes with graphite for simplification. Figure B-1 presents depletion result for both designs by imposing reflective boundary conditions. As expected, additional graphite increased the reactivity with difference on reactivity for about 700pcm throughout the beginning of life and significantly over estimated the reactivity at the middle of life with peak of 1445pcm. As the fuel reaching its end, the reactivity decreased gradually.

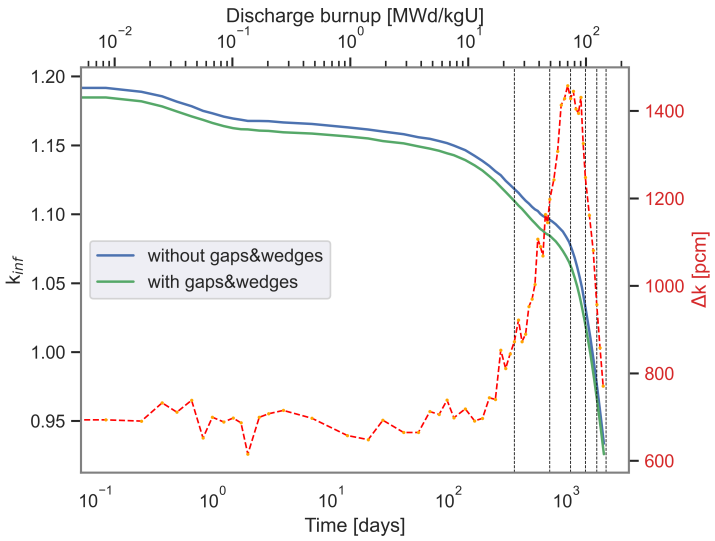


Figure B-1: Fuel assembly comparison with and without gaps

# Appendix C

# Figures

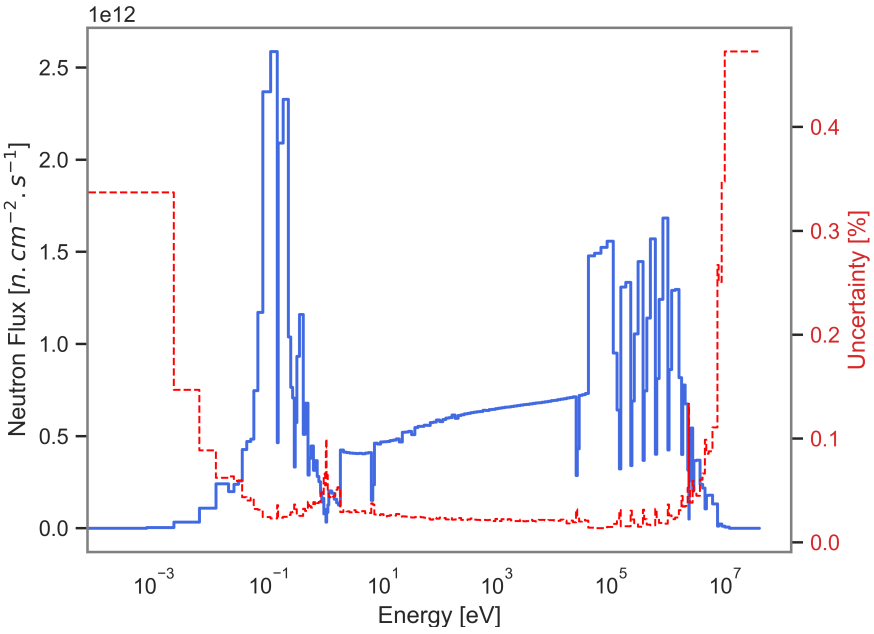


Figure C-1: Neutron spectra with 191 energy groups in fuel region for HC-HTGR using final control drums design

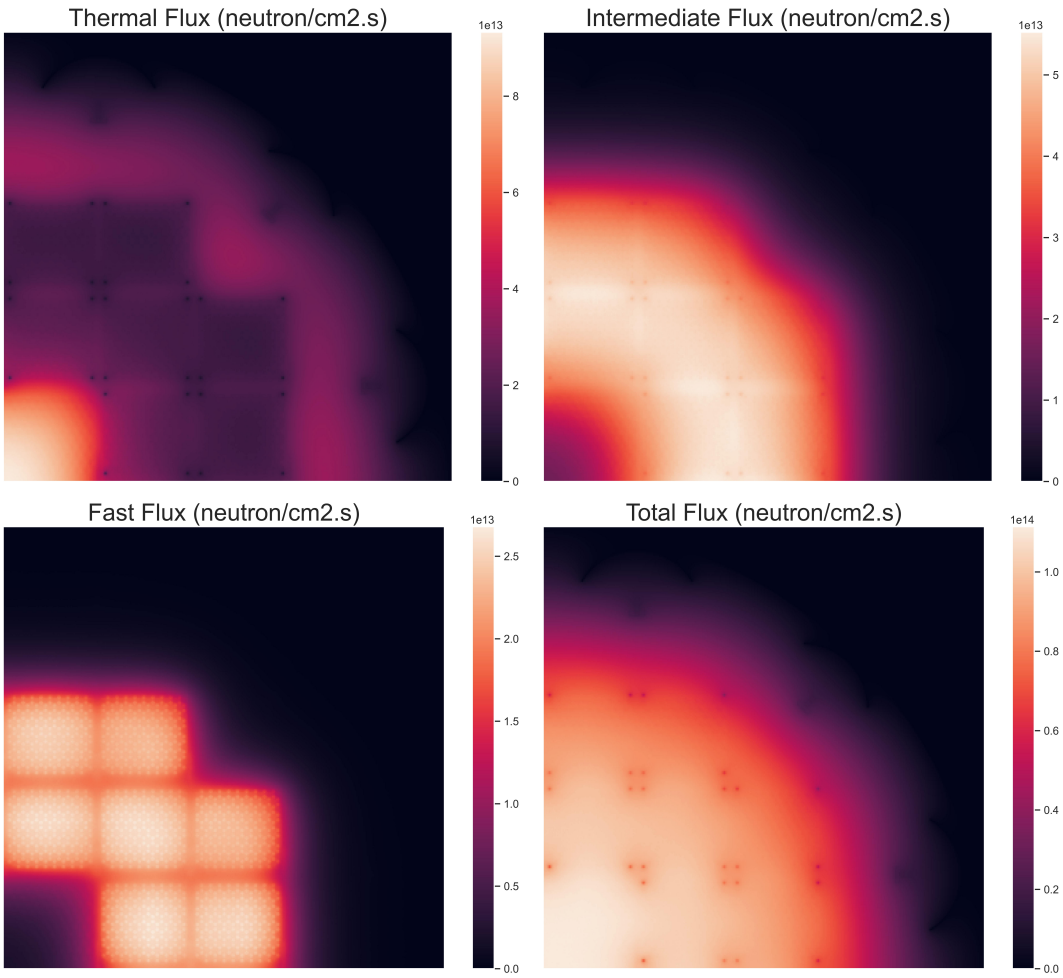


Figure C-2: Neutron flux for various energy groups for HC-HTGR using final control drums design

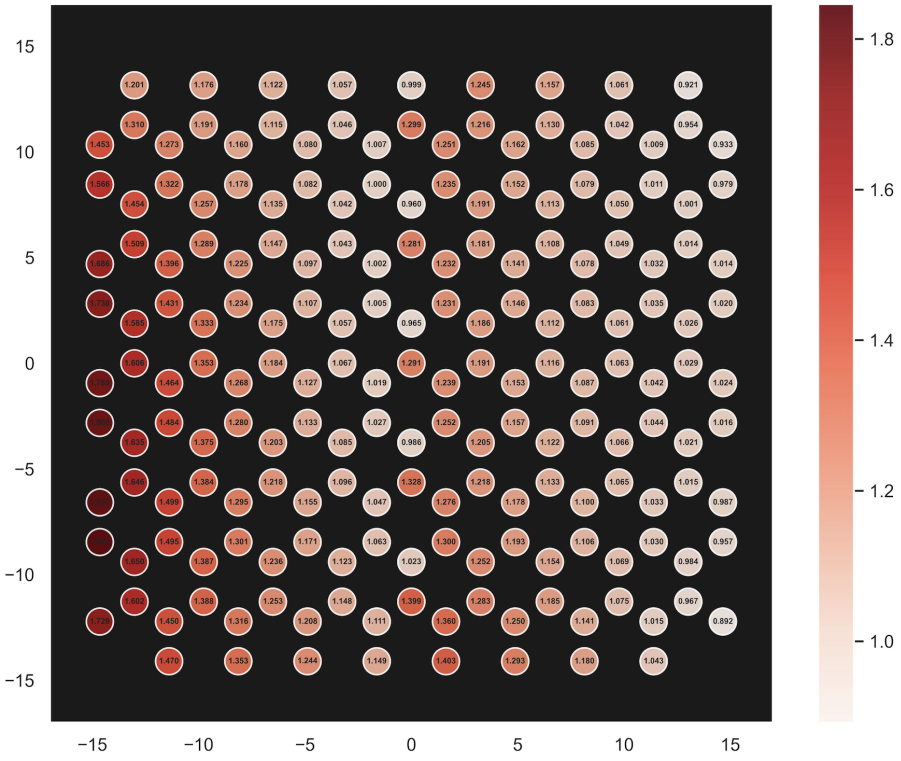


PPF uncertainty $< 0.7\%$

Figure C-3: 2D Radial pin PPF in core level during criticality for HC-HTGR using final control drums design

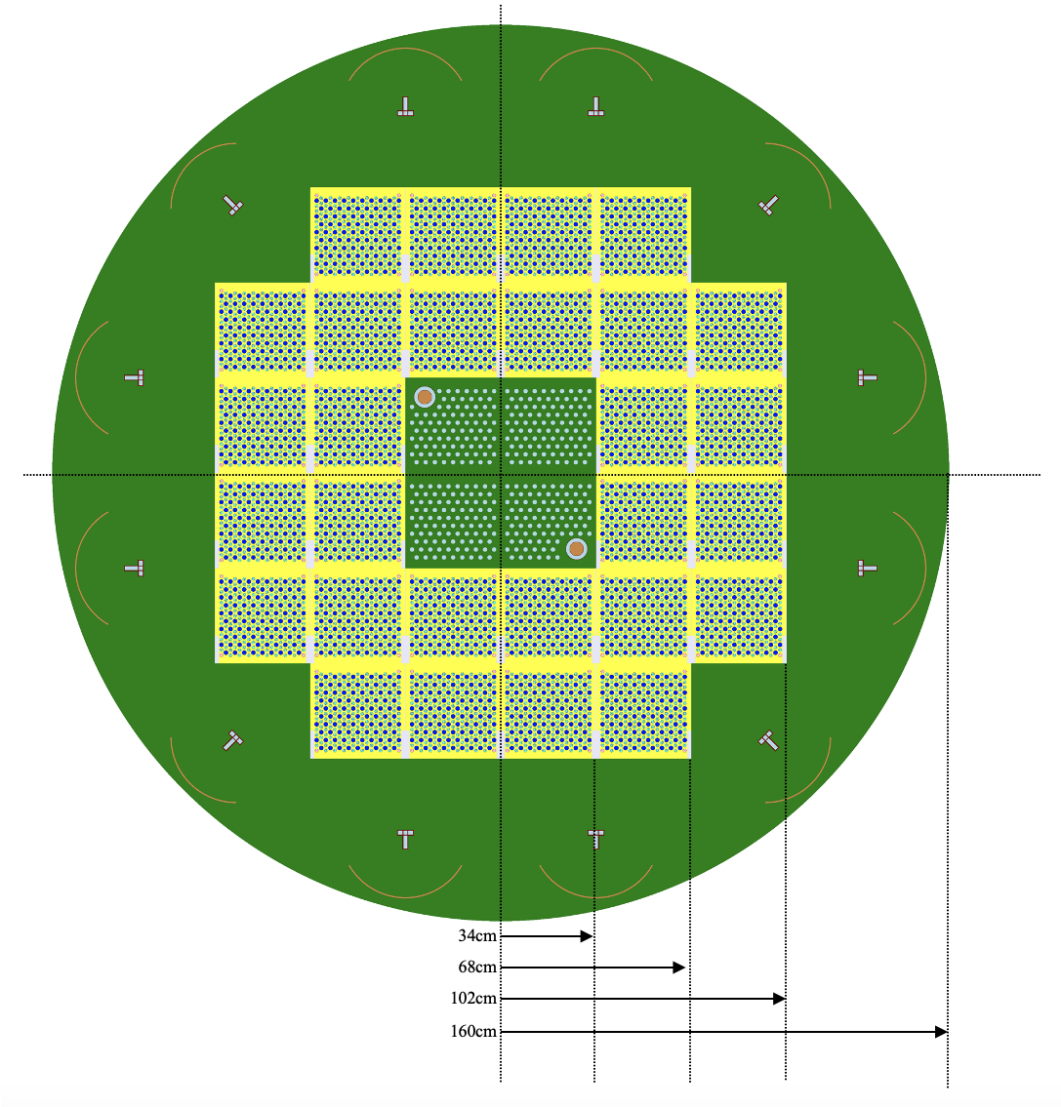


Figure C-4: HC-HTGR model with final control drums design and 2 inner control rods in radial view

# Appendix D

# Tables

Table D.1: Radius of r1m2 homogenization model

| **Fuel** | | **LBP** | |
|---|---|---|---|
| radius [cm] | material | radius [cm] | material |
| 0.39526 | Graphite matrix | 0.46312 | Graphite matrix |
| 0.41668 | oPyC | 0.47081 | PyC |
| 0.43143 | SiC | 0.47502 | Buffer |
| 0.44312 | iPyC | 0.48787 | $B_4C$ |
| 0.46374 | Buffer | 0.49193 | Buffer |
| 0.48187 | UCO | 0.49918 | PyC |
| 0.50089 | Buffer | 0.635 | Graphite matrix |
| 0.51100 | iPyC | | |
| 0.52310 | SiC | | |
| 0.53946 | oPyC | | |
| 0.635 | Graphite matrix | | |

Table D.2: Control drums with configuration E

| **Incoloy Thickness** [cm] | **CZPo** | **HFPo** | **HFPi** | $\Delta\rho_0$ [pcm] | $\Delta\rho_1$ [pcm] | **SDM** [%] |
|---|---|---|---|---|---|---|
| 0.3 | 1.16698 | 1.08528 | 0.98212 | 6451 | 9678 | 3.23 |
| 0.4 | 1.16640 | 1.08440 | 0.98230 | 6483 | 9585 | 3.10 |
| 0.5 | 1.16586 | 1.08381 | 0.98241 | 6494 | 9523 | 3.03 |

Table D.3: Control drums with configuration F

| **Incoloy Thickness** [cm] | **CZPo** | **HFPo** | **HFPi** | $\Delta\rho_0$ [pcm] | $\Delta\rho_1$ [pcm] | **SDM** [%] |
|---|---|---|---|---|---|---|
| 0.3 | 1.16471 | 1.08270 | 0.98226 | 6503 | 9444 | 2.94 |
| 0.4 | 1.16372 | 1.08183 | 0.98240 | 6505 | 9356 | 2.85 |
| 0.5 | 1.16316 | 1.08117 | 0.98222 | 6520 | 9318 | 2.80 |

Table D.4: Control drums with configuration G

| **Incoloy Thickness** [cm] | **CZPo** | **HFPo** | **HFPi** | $\Delta\rho_0$ [pcm] | $\Delta\rho_1$ [pcm] | **SDM** [%] |
|---|---|---|---|---|---|---|
| 0.3 | 1.16581 | 1.08411 | 0.98214 | 6464 | 9577 | 3.11 |
| 0.4 | 1.16499 | 1.08331 | 0.98222 | 6472 | 9501 | 3.03 |
| 0.5 | 1.16473 | 1.08259 | 0.98230 | 6514 | 9431 | 2.92 |

Table D.5: Control drums with configuration H

| **Incoloy Thickness** [cm] | **CZPo** | **HFPo** | **HFPi** | $\Delta\rho_0$ [pcm] | $\Delta\rho_1$ [pcm] | **SDM** [%] |
|---|---|---|---|---|---|---|
| 0.3 | 1.16384 | 1.08189 | 0.98213 | 6508 | 9389 | 2.88 |
| 0.4 | 1.16292 | 1.08104 | 0.98215 | 6513 | 9314 | 2.80 |
| 0.5 | 1.16228 | 1.08034 | 0.98232 | 6526 | 9236 | 2.71 |

Table D.6: Additional shutdown from cross hollow

| | **Incoloy Thickness** [cm] | **HFPo** [pcm] | **Worth** |
|---|---|---|---|
| Cross1 | 0.3 | 1.07711 | 699 |
| | 0.4 | 1.07777 | 567 |
| | 0.5 | 1.07803 | 495 |
| Cross2 | 0.3 | 1.07288 | 845 |
| | 0.4 | 1.07362 | 707 |
| | 0.5 | 1.07413 | 606 |
| Cross3 | 0.3 | 1.07536 | 751 |
| | 0.4 | 1.07595 | 631 |
| | 0.5 | 1.07661 | 513 |
| Cross4 | 0.3 | 1.07192 | 860 |
| | 0.4 | 1.07258 | 730 |
| | 0.5 | 1.07312 | 623 |

Table D.7: Control drums and 4 inner control rods

| **Rods length** [cm] | **Drums out** | $\boldsymbol{\Delta\rho_{out}}$ [pcm] | **Drums in** | $\boldsymbol{\Delta\rho_{in}}$ [pcm] | **SDM** [%] |
|---|---|---|---|---|---|
| | 1.15319 | | | | |
| 0.0 | 1.07321 | 6462 | 0.96585 | 10357 | 3.89 |
| 1.0 | 1.07285 | 31 | 0.96557 | 10387 | 3.92 |
| 2.0 | 1.07181 | 122 | 0.96442 | 10511 | 4.05 |
| 3.0 | 1.06996 | 283 | 0.96249 | 10719 | 4.26 |
| 4.0 | 1.06718 | 526 | 0.95999 | 10989 | 4.53 |
| 5.0 | 1.06303 | 892 | 0.95557 | 11471 | 5.01 |
| 6.0 | 1.05602 | 1517 | 0.94870 | 12229 | 5.77 |
| 7.0 | 1.04359 | 2645 | 0.93518 | 13753 | 7.29 |
| 8.0 | 1.01763 | 5089 | 0.90561 | 17244 | 10.78 |
| 9.4 | 0.98817 | 8019 | 0.84123 | 25695 | 19.23 |

Table D.8: Control drums and 4 inner control rods without outer incoloy

| **Rods length** [cm] | **Drums out** | $\Delta\rho_{\mathbf{out}}$ [pcm] | **Drums in** | $\Delta\rho_{\mathbf{in}}$ [pcm] | **SDM** [%] |
|---|---|---|---|---|---|
| | 1.16618 | | | | |
| 0.0 | 1.08441 | 6466 | 0.98098 | 9723 | 3.26 |
| 1.0 | 1.08384 | 48 | 0.98049 | 9774 | 3.31 |
| 2.0 | 1.08252 | 161 | 0.97915 | 9913 | 3.45 |
| 3.0 | 1.08102 | 289 | 0.97719 | 10118 | 3.65 |
| 4.0 | 1.07803 | 546 | 0.97452 | 10399 | 3.93 |
| 5.0 | 1.07375 | 916 | 0.96992 | 10885 | 4.42 |
| 6.0 | 1.06661 | 1539 | 0.96286 | 11641 | 5.18 |
| 7.0 | 1.05338 | 2716 | 0.94899 | 13159 | 6.69 |
| 8.0 | 1.02553 | 5295 | 0.91745 | 16782 | 10.32 |
| 9.4 | 0.98761 | 9039 | 0.84069 | 26734 | 20.27 |

Table D.9: Control drums and 2 inner control rods

| **Rods length** [cm] | **Drums out** | $\Delta\rho_{\mathbf{out}}$ [pcm] | **Drums in** | $\Delta\rho_{\mathbf{in}}$ [pcm] | **SDM** [%] |
|---|---|---|---|---|---|
| | 1.16020 | | | | |
| 0.0 | 1.07914 | 6474 | 0.97411 | 9991 | 3.52 |
| 1.0 | 1.07892 | 19 | 0.97384 | 10020 | 3.55 |
| 2.0 | 1.07824 | 77 | 0.97279 | 10131 | 3.66 |
| 3.0 | 1.07657 | 221 | 0.97116 | 10303 | 3.83 |
| 4.0 | 1.07406 | 438 | 0.96871 | 10564 | 4.09 |
| 5.0 | 1.07062 | 737 | 0.96532 | 10926 | 4.45 |
| 6.0 | 1.06481 | 1247 | 0.95914 | 11594 | 5.12 |
| 7.0 | 1.05528 | 2095 | 0.94876 | 12734 | 6.26 |
| 8.0 | 1.04044 | 3447 | 0.92802 | 15090 | 8.62 |
| 9.4 | 1.03204 | 4229 | 0.90897 | 17348 | 10.87 |

Table D.10: Control drums and 2 inner control rods without outer incoloy

| **Rods length** [cm] | **Drums out** | $\Delta\rho_{\mathbf{out}}$ [pcm] | **Drums in** | $\Delta\rho_{\mathbf{in}}$ [pcm] | **SDM** [%] |
|---|---|---|---|---|---|
| | 1.16636 | | | | |
| 0.0 | 1.08499 | 6430 | 0.98156 | 9712 | 3.28 |
| 1.0 | 1.08440 | 50 | 0.98126 | 9743 | 3.31 |
| 2.0 | 1.08358 | 120 | 0.98026 | 9847 | 3.42 |
| 3.0 | 1.08212 | 244 | 0.97865 | 10015 | 3.58 |
| 4.0 | 1.07959 | 461 | 0.97621 | 10270 | 3.84 |
| 5.0 | 1.07555 | 809 | 0.97248 | 10663 | 4.23 |
| 6.0 | 1.06968 | 1319 | 0.96608 | 11344 | 4.91 |
| 7.0 | 1.05964 | 2205 | 0.95505 | 12540 | 6.11 |
| 8.0 | 1.04276 | 3733 | 0.93313 | 14999 | 8.57 |
| 9.4 | 1.03219 | 4715 | 0.90866 | 17885 | 11.46 |

# Bibliography


[1] W. Stewart, E. Velez-Lopez, R. Wiser, and K. Shirvan, "Economic solution for low carbon process heat: A horizontal, compact high temperature gas reactor," *Applied Energy*, vol. 304, December 2021. https://doi.org/10.1016/j.apenergy.2021.117650.

[2] H. Goto, "High-temperature gas-cooled reactors and industrial heat applications," Nuclear Technology Development and Economics, Nuclear Energy Agency, 2022. https://www.oecd-nea.org/upload/docs/application/pdf/2022-06/7629_htgr.pdf.

[3] International Energy Agency, *Net Zero by 2050; a Roadmap for the Global Energy Sector*. https://www.iea.org/reports/net-zero-by-2050.

[4] United States Nuclear Regulatory Commission, *Nuclear Reactors, Power Reactors*. https://www.nrc.gov/reactors/power.html.

[5] Environmental Protection Agency, *"Inventory of U.S. Greenhouse Gas Emissions and Sinks: 1990-2018*. https://www.epa.gov/sites/default/files/2020-04/documents/us-ghg-inventory-2020-main-text.pdf.

[6] United States Nuclear Regulatory Commission, *Next Generation Nuclear Plant (NGNP)*. https://www.nrc.gov/reactors/new-reactors/advanced/licensing-activities/ngnp.html.

[7] J. M. Beck, and L. F. Pincock, "High temperature gas-cooled reactors lessons learned applicable to the next generation nuclear plant," INL/EXT-10-19329, Idaho National Laboratory, 2011. https://doi.org/10.2172/1023461.

[8] Nuclear Energy Agency, *Dragon Project*. https://www.oecd-nea.org/jcms/pl_51567/dragon-project.

[9] World Nuclear Association, *Peach Bottom 1, United States Of America*. https://www.world-nuclear.org/reactor/default.aspx/PEACH%20BOTTOM-1.

[10] P. Samanta, D. Diamond, and W. Horak, "NRC regulatory history of non-light water reactors (1950-2019)," BNL-211739-2019-INRE, Brookhaven National Laboratory, 2019. https://doi.org/10.2172/1579511.

[11] Office of Nuclear Energy, *TRISO Particles: The Most Robust Nuclear Fuel on Earth.* https://www.energy.gov/ne/articles/triso-particles-most-robust-nuclear-fuel-earth.

[12] World Nuclear Association, *Fort St. Vrain, United States Of America.* https://www.world-nuclear.org/reactor/default.aspx/FORT%20ST.%20VRAIN.

[13] Tsinghua University, *Status report 96 - High Temperature Gas Cooled Reactor - Pebble-Bed Module (HTR-PM).* https://aris.iaea.org/PDF/HTR-PM.pdf.

[14] General Atomics, *Prismatic coupled neutronics/thermal fluids transient benchmark of the MHTGR-350 MW core design.* https://art.inl.gov/NGNP/Water%20Ingress%20Assessment%20Review%20Material/INL%20Published%20Material/Preliminary%20Prismatic%20Coupled%20Neutronics%20Thermal%20Fluids%20Transient%20Benchmark%20of%20the%20MHTGR-350%20MW%20Core%20Design%2012-06-10.pdf.

[15] P. K. Romano, N. E. Horelik, B. R. Herman, A. G. Nelson, B. Forget, and K. Smith, "Openmc: A state-of-the-art monte carlo code for research and development," *Ann. Nucl. Energy*, vol. 82, August 2015. https://doi.org/10.1016/j.anucene.2014.07.048.

[16] P. Demkowicz, "Triso fuel: Design, manufacturing, and performance," NRC HTGR Training, Idaho National Laboratory, 2019. https://art.inl.gov/NRC%20Training%202019/04_TRISO_Fuel.pdf.

[17] N. E. Todreas and M. S. Kazimi, *Nuclear Systems.* Taylor & Francis, 2021.

[18] S. Glasstone and A. Sesonske, *Nuclear Reactor Engineering: Reactor Systems Engineering.* Springer Science & Business Media, 1994.

[19] L. Lommers and G. Honma, "Ngnp high temperature materials white paper," INL/EXT-09-17187, Idaho National Laboratory, 2012. https://doi.org/10.2172/1055953.

[20] B. J. Marsen, "Nuclear graphite for high temperature reactors," XA0103037, AEA Technology, 2001. https://inis.iaea.org/collection/NCLCollectionStore/_Public/32/047/32047840.pdf?r=1.

[21] L. Pengjun, Y. He, and D. Xingzhong, "Evaluation of the control rod super alloy material of htr-pm," *Proceedings of the HTR 2014*, October 2014. https://nucleus.iaea.org/sites/htgr-kb/HTR2014/Paper%20list/Track4/HTR2014-41199.pdf.

[22] S. Atkinson, T. Abram, D. Litskevich, and B. Merk, "Small modular high temperature reactor optimisation – part 1: A comparison between beryllium oxide and nuclear graphite in a small scale high temperature reactor," *Progress in Nuclear Energy*, March 2019. https://doi.org/10.1016/j.pnucene.2018.10.017.

[23] M. Abdullah, M. Arshad, S. Pervez, and K. M. Akhtar, "Beryllium reflector elements for parr-1," P1NSTECH-163, Pakistan Institute of Nuclear Science & Technology, 1999. https://inis.iaea.org/collection/NCLCollectionStore/_Public/31/037/31037765.pdf.

[24] A. L. Crawford, "Doe microreactor program: Control systems," GAINEPRINEI Microreactor Program Workshop, Idaho National Laboratory, 2020. https://gain.inl.gov/GAINEPRINEI_MicroreactorProgramVirtualWorkshopPres.

[25] T. M. Schriener and M. S. El-Genk, "Reactivity control options of space nuclear reactors," *Progress in Nuclear Energy*, April 2009. https://doi.org/10.1016/j.pnucene.2008.11.003.

[26] Y. Kim, K. Kim, and J. Noh, "Reactivity-equivalent physical transformation for homogenization of double-heterogeneous fuels," *Transactions of the Korean Nuclear Society Autumn Meeting*, October 2005. https://www.kns.org/files/pre_paper/17/84.pdf.

[27] L. Lou, X. Chai, D. Yao, X. Peng, L. Chen, M. Li, Y. Yu, and L. Wang, "Research of ring rpt method on spherical and cylindrical double-heterogeneous systems," *Ann. Nucl. Energy*, vol. 147, November 2020. https://doi.org/10.1016/j.anucene.2020.107741.

[28] J. Leppänen, M. Pusa, T. Viitanen, V. Valtavirta, and T. Kaltiaisenaho, "The serpent monte carlo code: Status, development and applications in 2013," *Ann. Nucl. Energy*, vol. 82, August 2015. http://dx.doi.org/10.1016/j.anucene.2014.08.024.

[29] P. E. MacDonald, J. W. Sterbentz, R. L. Sant, P. D. Bayless, R. R. Schultz, H. D. Gougar, R. L. Moore, A. M. Ougouag, and W. K. Terry, "Ngnp point design – results of the initial neutronics and thermal -hydraulic assessments during fy-03," INEEL/EXT-03-00870 Rev. 1, Idaho National Engineering and Environmental Laboratory, 2003. https://doi.org/10.2172/910732.